SYNTHESIS OF COMPOSITE PARTICLES BY DRY COATING TECHNIQUES

By

ALI ATA

A DISSERTATION PRESENTED TO THE GRADUATE SCHOOL
OF THE UNIVERSITY OF FLORIDA IN PARTIAL FULFILLMENT
OF THE REQUIREMENTS FOR THE DEGREE OF
DOCTOR OF PHILOSOPHY

UNIVERSITY OF FLORIDA

1998

A

ACKNOWLEDGMENTS

I would like to thank first my advisor, Dr. Rajiv K. Singh, for his guidance and support. His energetic and inspiring approach to research made my work enjoyable and meaningful. I want to acknowledge the Engineering Research Center for Particle Science and Technology for funding this research and providing a multidisciplinary and synergetic environment. The Engineering Particulate Thrust group meetings was very beneficial. I want to thank Dr. Yakov Rabinovich for his in depth discussions on surface forces which built up my basic knowledge on contact forces. Sincere thanks to Dr. Dinesh O. Shah for his valuable suggestions during thrust meetings and to Dr. Brij Moudgil for his encouragement and pressure to do more organized work. I would also like to thank Dr. Robert DeHoff, Dr. Jack Mecholsky, Dr. Laurie Gower and Dr. Bhavani Sankar for kindly participating on my dissertation committee. I appreciate Dr. Mecholsky for his effort in reading thesis in detail and giving valuable corrections.

I thank the people in Dr. Singh's group, Dr. D. Kumar, Dr. Dong Gu Lee, Uday, Kyu-Gong, Yalcin, Srini, Anu, Donald, David and Mark who made my stay pleasing by being always

respectful and friendly. Thanks are also given to James Fitz-Gerald for his sincere support in difficult times.

TABLE OF CONTENTS

ACKNOWLEDGMENTS ii

ABSTRACT iv

CHAPTERS

1 INTRODUCTION 1

Background and Motivation 1
Dissertation Outline 4

2 LITERATURE REVIEW 6

Introduction 6
Dry Synthesis Techniques 7
Powder Mixing 8
Rotary Mixer 11
High Speed Stirred Mixer 12
Mechanofusion System 13
Hybridization System 16
Particle Adhesion 17
Particle Size 19
Humidity 24
Surface Roughness 30
The Effect of Contact Deformation 37
Impact of Particles 43

3 EXPERIMENTAL APPROACH 68

Introduction 68
Description of MAIC System 69
Materials Used 71
Particle Loading 72
Particle Size 72
Processing Time 73
Humidity Studies 74
The Effect of Loading Force 77
Surface Roughness 78

Particle Movement and Velocity 80
Collision Frequency 81
Low Pressure and Vacuum Effects 82

4 RESULTS 95

Operating Parameters, Process Optimization 95
Processing Time 95
Current and Frequency 96
The Amount of Magnetic Particles 97
The Effect of Particle Size 97
The Effect of Humidity 98
The Effect of Loading Force 100
The Effect of Surface Roughness 101
The Effect of Low Pressures 104
The Role of Velocity 105
Collision Frequency 106

5 DISCUSSION 128

Composite Formation and Mechanism of the Process . 128
Particle Size Effect 130
The Effect of Humidity 132
The Effect of Loading Force 140
Surface Roughness Effect 144
The Role of Velocity of Particles 155

6 CONCLUSION 176

APPENDIX 178

REFERENCES 180

BIOGRAPHICAL SKETCH 185

Abstract of Dissertation Presented to the Graduate School of the University of Florida in Partial Fulfillment of the Requirements for the Degree of Doctor of Philosophy

SYNTHESIS OF COMPOSITE PARTICLES
BY DRY COATING TECHNIQUES

By

Ali Ata

December, 1998

Chairperson: Rajiv K. Singh
Major Department: Materials Science and Engineering

Composite particles were synthesized by a dry type technique called the magnetically assisted impaction coating (MAIC) process. The MAIC process is a collision based process where magnetic particles are used to fluidize the powder mixture containing submicron sized secondary particles and large primary particles. Primary particles are coated as a result of impaction taking place in the system between the particles.

Due to their small sizes, secondary particles tend to agglomerate. Minimization of cohesive forces causing agglomeration and promoting adhesive forces is a major challenge in all dry coating systems. In order to overcome

the problem of agglomeration, factors influencing adhesion were studied. Particle size, humidity, surface roughness, plastic deformation, and velocity of particles are among the major parameters playing important role in adhesion.

The characterization of surface coating was done by scanning electron microscopy (SEM). Adhesion forces were characterized by atomic force microscopy (AFM).

The efficiency of coating was observed to increase as the size of secondary particles decrease in particular below 0.4 μm. A critical humidity range near 60% relative humidity resulted in poor surface coverage by formation of liquid bridges among particles, which causes excessive agglomeration. The adhesive force was observed to drop sharply within 1-2 nm root mean square (RMS) roughness change. The existence of plastic deformation at the contact region increased adhesion forces.

CHAPTER 1
INTRODUCTION

Background and Motivation

Composite particles have a wide range of applications such as in the ceramic industry, the pharmaceutical industry, in metal hydride based rechargeable batteries, and so on. Some major applications are listed in table 1 [Nai93a].

The methods used to synthesize composite particles can be classified into three categories: wet, vapor and dry phase techniques. The wet chemical techniques include sol gel, precipitation and coagulation [Wan96, Har92] electroplating [Sug98]. However, these methods require an aqueous solution and the treatment of the waste liquid sometimes causes serious pollution problems. Chemical vapor deposition, physical vapor deposition, sputtering and laser ablation are examples of gas phase methods [Kaa95]. These techniques involve expensive gas equipment and vacuum systems and some of them show poor adhesion [Sug98]. Dry techniques using mechanical methods to form composite particles, emerged as a viable technique primarily during the 1990s.

Table 1-1. Applications of composite powders.

Application Field	Core Particle	Fine Particle	Function
Medicine	Aspirin Granule (20-32 Mesh)	Carnauba (15 μm)	Release control of aspirin
Cosmetics	Polyethylene (12 μm) Nylon sphere	TiO_2 (1 μm) TiO_2	Coloring Covering from UV-Light
Toner	Resin (3-25 μm)	Pigment	Photocopy
Conductive Resins	PMMA (50 μm)	Ag (1 μm)	Forming a network of conductive paths in bulk materia
Metal/Ceramics Composite Materials	Al-alloy powder (30-60 μm) SS-316L (3 μm)	Y_2O_3 (3 μm) 3Y-PSZ (0.3 μm)	Interface layer between substrate and thermal spray layer Good uniformity for sintering
Filler	MgO	Fatty acid	Surface reforming of MgO from hydrophilic to hydrophobic
Solid Lubricant	Inorganic Powder	Polymer	Composite solid lubricant
Contact Materials	Ag-Ni Alloy (210 μm)	Ni (1 μm)	Rivets

The advantages of dry techniques are the formation of uniform coatings without a solvent or binder, low production cost, easy operation, reduced waste and short processing times. Various mechanical forces, such as shear, compressive, impact are applied to a powder mixture composed of primary and secondary particles. Secondary particles are fine sized, generally in the submicron range, while primary particles are large particles ranging from tens of microns to millimeter

sizes. As a result of mechanical action, small secondary particles are attached or adhered to large primary particle surfaces forming composite powders. The process is shown schematically in figure 1-1.

Submicron sized particles exhibit more violent Brownian motion in air and thus are agglomerated. The major challenge in any dry coating system is to break agglomerated secondary particles. Conventional grinding or mixing techniques are no longer sufficient to disperse and minimize the size of agglomerates efficiently. Due to this limitation, during 1987, a shear compression type machine called the mechanofusion system was developed [Miz91] to obtain composite particles. Recently, another technique called the hybridization system using premixed powder was developed [Ono89].

Although there is an industrial demand for composite particles, fundamental research toward understanding the effective parameters in composite formation does not exist. An in-depth investigation of adhesion and agglomeration aspects of dry synthesis of composite particles is the motivation behind this research. Development of a novel technique called the magnetically assisted impaction coating (MAIC) process is also an objective of the study.

Dissertation Outline

The objective of this research is to investigate parameters effective in synthesis of composite particles by dry techniques as well as understanding the fundamentals of adhesion of particles with a surface in dry environments. A novel technique called the magnetically assisted impaction coating (MAIC) process was used to synthesize composite particles.

Chapter 2 gives a general review on the subject of composite particles, their industrial applications, processing techniques, the mechanism of formation, and effective parameters influencing the composite formation including relevant aspects of particle adhesion.

Chapter 3 includes the experimental procedure used in this study. Chapter 4 presents the results of the experiments, followed by a discussion of the results in Chapter 5. The conclusion of the study is given in Chapter 6.

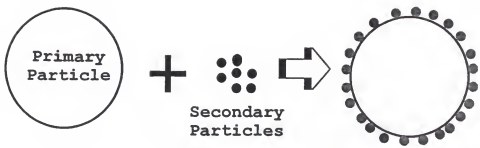

Figure 1-1. The schematic description of composite particle synthesis in dry systems.

CHAPTER 2
LITERATURE REVIEW

Introduction

In this chapter, the relevant studies about the major variables controlling the composite particle formation in dry environments will be presented starting with a short description of the existing dry synthesis techniques.

Current research has been focusing to improve the physical and mechanical characteristics of composite particles. The adhesion of particles as well as agglomeration during coating are fundamental issues that need to be addressed in further details.

The major parameters affecting the composite formation or adhesion of secondary particles to primary particles can be listed as particle size, humidity, plasticity of the interacting particles, surface roughness, pressure level inside the processing unit, fluidization of powder mixture or mixing, and velocity of interacting particles.

Dry Synthesis Techniques

In any powder coating system, the particle size of the coating agent (secondary particles) is much smaller than that of the particles to be coated. Accordingly, the amount of secondary particles required to form a mono-layer on the primary particle surface is very small. In addition, the secondary particles are in agglomerated form. This means that in the beginning, when the system is completely in unmixed state, the secondary particles are distributed in lumps within the bulk and there exist large zones of the chamber with no secondary particles at all. Therefore, the first requirement in dry systems is the reduction of the size of those zones. In other words, a well-mixed state is necessary for the secondary particles to reach and come into contact with all of the primary particles. The dispersion of secondaries depends on the strength of the forces imparted to the powder mixture.

Comminution or grinding-based techniques have been a useful method to impart an effective force on the surface of particles and hence to produce composite particles. Almost every fine grinding machine that appears new on the market appeals by its ability to make various kinds of composite particles, aside from its function of efficient grinding

[Nai93a]. Table 2-1 shows the main grinding machines which have been applied for composite particle formation.

Table 2-1. Grinding machines used in synthesis of composite particles.

Class	Types
Impaction	Pin Mill, Disc Mill
Ball Mill	Rotation, Vibration, Planetary, Jet Mill
Attrition	

Another common way to synthesize composite powders is mixing but the methods are inevitably accompanied by agglomeration. To overcome the agglomeration problem, mixers with higher mechanical energy input have been required for dry coating systems. Advanced dry coating systems based on mechanical principles such as mechanofusion and hybridization have been recently developed for this purpose.

Powder Mixing

Powder mixing has been the subject of numerous investigations. Most of the systems examined consisted of relatively coarse, free flowing particles and lead to the concept of randomization of the particles. The randomization may be brought about by a variety of mechanisms including diffusion and convection, according to the type of mixer employed. Randomization requires equally sized and weighed

particles, with little or no surface effects, showing no cohesion or interparticle interaction [Her79]. When the powders adhere together during the mixing operation, especially for cohesive or interacting particulate systems, they will form an ordered mixture.

There is no theoretical reason why fine, secondary particles cannot be mixed by the randomization process. However, cohesive properties and other surface phenomena usually develop with increasing fineness and these will tend to order rather than to randomize the mixing operation. When there is large difference in particle size, particles would tend to segregate at a faster rate than they would mix together. Particle interaction, that is, adsorption, chemisorption, surface tension, or frictional, electrostatic or any other form of adhesion results in an ordered mixing arrangement of the particles which is shown in figure 2-1(a) for an equal mixture of black and white particles. Figure 2-1(b) shows the same mixture in a randomized pattern.

Mixing mechanisms can be classified into three categories [Lac54]:

1-diffusive mixing, which occurs when particles roll down a sloping surface;

2-shear mixing, which occurs when slip zones are established in a powder; and

3-convective mixing, which occurs when circulation patterns are set up inside a bulk powder mass.

When particles which have no tendency to segregate are mixed these three mechanisms are all effective.

Generally more than one of these three effects will be present in mixing but usually one of the mechanisms predominates in a given system.

Any mixer which relies on a tumbling motion, that is, one in which the particles are in a rotating container, is mainly using diffusive mixing. When making composite particles from free flowing particles of different size, there will be a large amount of segregation, which will severely limit the quality of mixing [Kay97]. Systems which rely on a stirring action, not accompanied by much convective or shear motion, will also produce an appreciable amount of segregation and therefore will not be suitable for composite formation.

In order to disperse particles which are too cohesive like secondary particles, the main requirement is that the system should provide sufficient shear forces to break up the agglomerates.

Rotary Mixer

The mixer is a cylindrical vessel equipped with three baffles and performs a rocking movement in the axial direction while rotating as shown in figure 2-2 [Alo88]. The rocking

angle is set at 20° except for the experiments run without rocking in which the mixer was rotated in the horizontal position.

As soon as the mixer is set in motion, by collision, friction and shearing, the secondary particles are distributed randomly throughout the mixer. The rotation movement of the vessel assures complete radial macro-mixing randomly distributing the coated and non-coated particles at any section of the vessel. Figure 2-3 [Alo89a] shows the influence of rotation and rocking speeds on the mixing time. The materials used in the experiment were white glass powder of 350 μm diameter and secondary particles of black dye. N is the rotation speed and N_c is the critical rotation speed based on the inner diameter of the cylinder (N_c=80 rev/min). It is readily noticed that the rocking-promoted convective motion of the powder greatly enhances the rate of mixing, which is very low when only rotation (diffusive mixing) is imparted to the mixer. Furthermore, at high rocking speeds the effect of increasing the rotation speed is practically negligible and somewhat striking; to a certain extent, the lower rotation speeds give the shorter mixing times. It is concluded that rotational movement of the mixer generates shearing and friction forces which exert a strong and positive effect on the rate of coating, and rocking motion facilitates and

accelerates the mixing of cohesionless and non-segregating materials.

High Speed Stirred Mixer

The mixer is a round-cornered conical bottomed cylindrical vessel with an impeller that rotates at rather high speeds as shown in figure 2-4 [Alo89b]. Initially, the secondary particles are equally distributed along the axial direction of the cylinder by placing constant amounts of powder. This assures rapid axial macro-mixing of the components, whereas radial mixing is achieved due to impellers' motion. Simultaneously with the rotating motion of the impeller, the vessel is vibrated in the three spatial directions, with a frequency of 33.3 Hz, by an unbalanced electric motor drive. Both the design of the bottom and the vibrations applied to the vessel prevent the formation of stagnant or dead zones within the mixture. The temperature of the mixture was measured by a thermometer inserted into the powder bed.

Direct observation of the early stages of mixing shows that the aggregates of fines attach to the coarse particles in their neighborhood and these so-formed carriers distribute the fine component throughout the bulk of the bed. The creation of new carriers by the transfer of fines from coated to non-coated particles follows the kinetics of a second order

autocatalytic chemical reaction. The rate at which the agglomerates are broken up is a function of the intensity of the shearing force generated in the mixer. It is seen that the expected enhancement of the powder flowability at low concentrations and increasing agitation speeds becomes appreciable only after long mixing times.

The introduction of large shear forces may in some cases lead to the fracture of particles; if this cannot be tolerated then systems with high-speed impellers should be excluded.

Mechanofusion System

The outline of the experimental apparatus is shown in figure 2-5 [Nai93b]. The main part consists of a rotating chamber and a semi-cylindrical arm head fixed with a certain clearance against the inner surface by centrifugal force and receives the complicated forces such as compression, shearing and rolling between the arm head and inner surface of the chamber. Providing a sufficiently narrow gap between the inner arm head and the inner wall of the rotary vessel allows the particles passing through this gap to violently collide with each other, thereby generating enough heat energy to fuse the particles together. The powder subjected to this action is scraped off from the inner surface by the scraper and again subjected to the above action. It is expected that the composite particles are obtained by repeating this action

during processing. In setting the experimental conditions, the combinations of particles and mixing ratio are defined while for the operation conditions, rotation speed of the apparatus, atmosphere, temperature and such are determined.

In the experiment [Nai93b], glass primary particles of 23 μm size and titanium dioxide of 0.015 μm were weighed for the specified ratio and a total of 500 grams of the particles was loaded in the chamber and rotated at the set speed (500-1000 rpm) for the specified time. The change of the ratio of secondary particles fixed onto the surface of glass beads was observed as a function of processing time. The ratio increases with time and becomes constant at 0.9 in five minutes or more for 500 rpm.

Temperature varied with rotation speed and attained the highest speed approximately within 5 min when there is no water cooling. The measured temperature represents a rough average. The actual local temperature on the particle surfaces was significantly higher when the effect of thermal conduction was taken into account [Tan90].

Composite forming consists of the following steps [Tan90]:

1-A strong shear stress created in front of the inner piece acts on the agglomerated guest particles to divide them into mono-dispersed, smaller agglomerates.

2-The strong compressive and impact forces created in a narrow space force the secondary particles to adhere to the primary particle surface by mechano-chemical reactions.

3-The heat energy generated by the collision of particles increases the temperature of the minute surfaces of the secondary particles. This, coupled with the compressive force acting on the particles, causes re-agglomeration of the particles. At the same time, friction between the particles causes the core particles to rotate, rolling the reagglomerated particles onto them to form a coating layer of secondary particles on each of the core particles.

4-The secondary particles are bonded to each other by sintering, and the sintering accelerates, spreading throughout the agglomerated secondary particles.

5-The solidified layer propagates throughout the coating layer to form a shell encasing each of the primary particles.

Most oxides in solid states have long been considered stable against chemical reactions as long as they are treated in a dry environment at room temperature. However, once mechanical stress is applied on these solids or particularly on a solid mixture, this is no longer the case [Sen97].

Mechanochemical interaction between dissimilar solids is often demonstrated by quick dehydration, amorphization and chemical shift of the binding energy of core electrons detected by X-ray photoelectron spectroscopy (XPS). This kind

of interaction is supported by a high resolution transmission electron microscope (HRTEM), by which some crystallites are observed in a mixture after ball-milling for quite a short time [Kom94].

Hybridization System

In this system, syntheses of composite particles are achieved by means of embedding or filming one powder onto another. The system first prepares an ordered mixture in a separate section by premixing the secondary and primary particles and consists of O.M'izer (where the ordered mixture is prepared), hybridizer, collector and control panel. The ordered mixture is weighed and simultaneously fed into the hybridizer. The hybridizer disperses the powders in the gaseous phase, transmitting mechanical and thermal energy due to rotation and mixing, allowing particle coating by embedding and filming. Very short processing times of 1-5 minutes are required for optimum coating. A schematic of the hybridizer system is shown in figure 2-6. Commercially, the hybridizer is being used in the cosmetic, paint, toner, food and pharmaceutical industry.

Particle Adhesion

Hersey [Her75] considers the influence of adhesion in powder mixing, but he does not complement his theory by an adhesion measurement. Schmidt and Walter [Sch94] tried to link the adhesion between the particles in a powder bulk to the mixing properties, but their method of measuring adhesion forces is not sensitive for fine secondary particles and the values measured were always bulk values instead of adhesion force values for single particles. However, the adhesion between individual particles of the powder bulk is the main factor involved and needs to be quantified for a fundamental understanding of powder behavior during processing.

Particle adhesion is the result of forces which exist between particles and a solid surface in contact, where the solid surface itself can be a particle surface such as a primary particle.

The attractive interaction forces between different media include all those types of interaction that contribute to the cohesion of solids, such as metallic, covalent and ionic (primary chemical bonds), as well as secondary van der Waals bonds. The energy of a primary bond is of the order of a few electron volts, that of a secondary bond about 0.1 eV. In addition there are interaction forces of intermediate energy such as hydrogen bonds, electronic charge transfer bonds and

electrostatic double layer forces. These various interactions can be classified into three categories as follows [Kru67]:

1-long range attractive interactions that prevail in the region of contact and in the peripheral area such as van der Waals and electrostatic forces,

2-short range attractive interactions that result from chemical bonding as well as intermediate energy bonding such as hydrogen bonding, and

3-the adhesion forces caused by interfacial reactions such as diffusion, condensation and diffusive mixing.

It appears that classes 1 and 3 are of primary importance to particle adhesion because they determine the size of adhesive area whereas contributions from class 2 to the overall adhesive strength can only result if an adhesive area of finite size has already been established by the interactions of class 1 and 3.

At room temperature or below, the interfacial reactions of class 3 are not likely to occur. As a first approximation of particle-substrate adhesion, class 2 interactions can be disregarded because, except under extraordinary conditions of purity under, say, an ultrahigh vacuum, primary chemical bonds at the surfaces will tend to become saturated from contamination. They will then be no longer available to chemical interactions with other particles. As a result, the main forces involved in particle adhesion are van der Waals,

electrostatic and capillary forces. The magnitude and type of force depend on the properties of the materials which are in contact, and the ambient environmental conditions. The most crucial ones can be listed as

1-Particle size,

2-Relative humidity,

3-Surface roughness, and

4-Viscoelastic/Plastic behavior of the contiguous bodies.

These parameters are studied and elaborated in the following sections together with the velocity and low pressure effects.

Particle Size

In general, the primary contribution for microscopic particles adhering to solid surfaces in dry systems is attributed to van der Waals forces [Bow88]. According to van der Waals' theory, the total adhesion force on a particle increases linearly as the size of the particle increases. The adhesion force change as a function of the diameter of the particle is expressed as

$$F = \frac{AR}{6Z^2} \tag{2.1}$$

where, A is the Hamaker constant, R is the radius of the

particle, and Z is the intermolecular separation distance between two bodies usually taken as 0.3 nm.

The van der Waals forces are only noticeable when the particles can come sufficiently close together, that is, at separation distances of the order of the size of a molecule, 0.2 to 1 nm. Moreover, their magnitude becomes negligible compared with that of the gravitational force when the particle size exceeds a certain value. This value is of the order of a few microns as shown in figure 2-7.

The van der Waals force is a consequence of the general attraction between molecules. The Dutch physicist van der Waals explained that the deviations from the ideal gas law at high pressures could be caused by molecules in a gas attracting each other [Vis89]. It was only after the development of the theory of quantum mechanics that London, almost 60 years later, in 1930, could quantify van der Waals' hypothesis.

Van der Waals forces have three components: (1) dipole-dipole interactions, (2) dipole-nonpolar interactions, and (3) interactions between nonpolar bodies or dispersion components [Don93]. The dispersion effect is the major contribution to the intermolecular forces except when the polarizability is small and the dipole moment is large [Cor66]. The forces are additive for assemblies of atoms or molecules. Atoms or

molecules may be characterized at each moment by an attractive force. This force results from the short period movement of the electrons in the atoms or molecules giving rise to dipoles, which change continually in magnitude and direction. At each moment an attractive force exists between the induced and inducing dipoles. By a quantum mechanical treatment of this phenomenon, London obtained the following equation for the mutual attraction energy "V" between two molecules with polarizability α, a characteristic frequency ν_0 and separation distance "z":

$$V=-3/4h\ \nu_0 \alpha^2/z^6 \qquad (2.2)$$

where h is Planck's constant. Since ν_0 is found in the ultraviolet region of the total absorption spectrum, and hence plays an important part in optical dispersion, the intermolecular London-van der Waals forces are also named dispersion forces.

The attractive force decreases rapidly with distance of separation, but is effective within several molecular diameters. For evaluating the van der Waals force, microscopic and macroscopic approaches were used [Sol94]. The microscopic approach was based on the interactions of the individual molecules and was calculated by integration over all pairs of atoms and molecules. Bradley [Bra36] and Hamaker [Ham37] carried out this integration using the expression

$\Phi=-\lambda/r^6$ to describe the van der Waals' attractive potential between two molecules separated by a distance r, where λ is the van der Waals' constant. They calculated the attractive potential between two spheres considering the additivity of the interactions as follows:

$$E=-\int\lambda/r^6 n_1 dV_1 n_2 dV_2 \qquad (2.3)$$

where V_1 and V_2 are the volumes of the spheres and n_1dV_1 is the number of molecules in volume element dV_1 separated by r from the n_2dV_2 molecules in volume element dV_2. The resulting van der Waals attractive force between a particle and a surface is given in equation (2.1).

The Hamaker theory is deficient in a number of respects, chief of which is the assumption of "pairwise additivity." If one considers the interaction between two atoms or molecules in the presence of other atoms, the instantaneous field due to atom 1 not only induces a dipole in atom 2 but also in other atoms, which in turn act on atom 2 [Sev97]. The macroscopic approach developed by Lifshitz [Lif56] in 1956 avoids the problem of additivity by ignoring the atomic structure of the bodies and treating them as continua. Therefore, the Lifshitz theory is physically more satisfactory dealing directly with the bulk properties of the interacting bodies. The van der Waals attractions between two solid bodies are calculated from the imaginary parts of their complex dielectric constants by

solving Maxwell's electromagnetic equations [Tsa91].

According to the Lifshitz approach, the force between a particle and a surface is given as

$$F = \frac{\hbar\varpi R}{16\pi Z^2} \tag{2.4}$$

where $\hbar\varpi$ is the Lifshitz-VdW constant, which ranges between 1 and 10 eV depending on the materials in contact. The Lifshitz-VdW constant is related to the Hamaker constant by

$$A = \frac{3}{4\pi}\hbar\varpi \ . \tag{2.5}$$

Some typical values of $\hbar\varpi$ are given in table 2-2.

Table 2-2. $\hbar\varpi$ values for some systems in vacuum and in water.

Combination	$\hbar\varpi$ in vacuum	$\hbar\varpi$ in Water
Au-Au	14.3	9.85
Ag-Ag	11.7	7.76
Cu-Cu	8.03	4.68
C-C	8.60	3.95
Si-Si	6.76	3.49
Ge-Ge	8.36	4.66
MgO-MgO	3.03	0.47
Al2O3-Al2O3	4.68	1.16
Polystyrene-Polystyrene	1.91	0.11

In dealing with the mechanical interaction between different materials, such as primary and secondary particle interactions, the Hamaker or Lifshitz-van der Waals interaction coefficient A_{12} can be obtained to a good approximation by taking the geometric mean of the individual coefficients A_{11} and A_{22} [Vis89]:

$$A_{12} = \sqrt{A_{11}A_{22}} \,. \tag{2.6}$$

Humidity

When considering the adhesion of particles in air, it is easy to overlook or underestimate the important role of capillary forces resulting from humidity. Adhesion between particles in air usually increases as the relative humidity of the ambient air is increased. However, capillary adhesion of a particle to a surface is a conditional adhesive force of importance for two reasons: (1) its magnitude can exceed the van der Waals force, and (2) it varies as the first power of particle diameter. If a film of liquid exists between a particle and a surface in contact, and if the radius of the film at the contact point is small relative to the radius of the particle, 'R', the force of adhesion due to the liquid film in an inert atmosphere is [Isr85]

$$F = 4\pi R\gamma \tag{2.7}$$

where γ is the surface tension of the film. Equation 2.7 is applicable to perfectly smooth surfaces and represents the maximum force which could be experienced as a result of the liquid layer. In practice the force of adhesion approaches that predicted value of equation only at relative humidities close to 100%.

The adhesion force in an atmosphere containing a condensable vapor, the above equation is replaced by [Ran87]

$$F = 4\pi R[\gamma_{LV}\cos\theta + \gamma_{SL}] \tag{2.8}$$

where the first term is due to the Laplace pressure of the meniscus and the second is due to the direct adhesion of the two contacting solid surfaces within the liquid.

Israelachvili and Fisher [Isr85] expressed the adhesion force equation between similar spheres of radius R and flat surface with the same contact angle θ, as follows:

$$F = 4\pi\gamma R[\cos\theta + 0.5\sin 2\phi \sin(\theta + 2\phi)] \tag{2.9}$$

where 2ϕ is the angle embracing meniscus as shown in figure 2-8. The second term in this formula can be usually neglected because usually R>>r.

Note that the above equation does not contain the radius of curvature r of the liquid meniscus as shown in figure 2-8.

This is because for smaller r the Laplace pressure γ_{LV}/r increases but the area over which it acts decreases by the same amount, so the two effects cancel out [Isr92]. For small values of γ_{SL} such as the case for organic liquids (relative vapor pressure=0.1-0.2), the adhesion is mainly determined by the $\gamma_{LV}\cos\theta$ term. In that case, only at meniscus radii below about 5Å (corresponding approximately to the sizes of the organic molecules) does the adhesion force deviates abruptly from the bulk value, tending to the value of the dry system (relative vapor pressure=0). The behavior with water is completely different: there it is found [Isr82] that the adhesion force was given by equation (2.7) only at relative vapor pressure above 0.9, that is, the radius of the meniscus above 50 Å. At lower relative vapor pressures, the adhesion force falls toward the dry state limit. It is concluded therefore that all the liquid condensates manifest their bulk thermodynamic properties above some meniscus radius. For organic liquids this critical meniscus radius is of the order of the sizes of the molecules, while for water it is much larger of the order of 20 molecule diameters reflecting perhaps the long-range nature of the cooperative hydrogen-bonded interaction in water that gives rise to its bulk surface properties, such as, surface tension [Isr82].

A liquid bridge has a curved surface, and therefore the

pressure on both sides of the surface is not, in general, the same, the pressure difference ΔP is given by the Laplace-Young equation

$$\Delta P=\gamma_L[1/r_1+1/r_2] \tag{2.10}$$

where γ_L is the surface tension of the liquid and r_1, r_2 the radii of curvature of the surface measured in two planes at right angles to each other. Since $r_2>>r_1$, $\Delta P=\gamma_L/r_1$. The Laplace pressure acts on an area $\pi x^2\approx 2\pi Rd$. The distance d and x are given in figure 2-8.

The adhesion force is

$$F_{ad}=\Delta P x S \tag{2.11}$$

where S is the area of flat plate coated by condensed water. S can be calculated by the formula

$$S=2\pi Rr(\cos\theta_1+\cos\theta_2). \tag{2.12}$$

Substituting equation (2.12) in (2.11) gives a general expression for adhesion force in dissimilar solids:

$$F_{ad}=2\pi\gamma R(\cos\theta_1+\cos\theta_2). \tag{2.13}$$

The capillary force can make a large contribution to the total force of adhesion. There is evidence that a capillary force may remain even after baking for as long as 24 hr [Bha78]. If the liquid contains substances that can crystallize upon evaporation, a solid crystalline bridge might also form during drying. Solid bridges do not play an

important role in dry powder processing or bulk flow [Pod94]. It should be pointed out that hydrophobic surfaces are not generally affected by capillary forces [Bow85]. Figure 2-9 shows the magnitude of a capillary force in comparison to the van der Waals forces for "A" equal to 5 eV. It can be seen that the capillary force is about four times as large as van der Waals forces which are by an order of magnitude greater than electrostatic adhesion forces between conductors [Rum78].

Zimon [Zim82] showed, between 5-65% relative humidity, that with a given removal force there was little change in the adhesion number, Y_F, defined as the percentage of particles remaining on the surface, but in the 65-100% range the adhesion number increased rapidly as shown in figure 2-10. Zimon also found a hysteresis loop that is the adhesion number at any given humidity was different when relative humidity was rising and falling as shown in figure 2-11. The presence of adhesion hysteresis was thought to be indicative of the ambiguous nature of the capillary condensation and moisture evaporation processes in the gap between the contacting bodies, and apparently associated with the special properties of thin liquid layers in capillaries [Zim63].

Experiments with quartz particles of different sizes in air at relative humidity approaching 100% were conducted [Cor66]. The results are shown in figure 2-12. The majority

of particles were held with forces less than that predicted by equation (2.6) Corn suggested that the increased adhesion between quartz particles was related to the water adsorption characteristics of quartz. The adsorbed layers may be considered as part of the particles and a decrease in the inter-particle distance will thus occur, causing the van der Waals forces to increase [Coe78].

As the amount of water adsorbed on the contacting surfaces increases, the interparticulate contacting area increases, and the powder gradually becomes more cohesive. A gradual change of this nature can usually be accommodated within an industrial process [Har96a]. Unfortunately, for many industrial powders the change is not gradual but at a "critical" relative humidity the distribution of the surface moisture changes from that of adsorbed surface molecules to that of a flexible liquid bridge holding particles together.

Work on loose bulk powders has indicated that a small change in relative humidity can produce substantial changes in the processing characteristics of the powders. Harnby [Har82] has shown that resultant changes in the flow characteristics of a powder mixture can have a marked effect on powder mixture quality. Hartholt et al. [Har96b] reported that when the relative humidity of the fluidization gas was increased from 45% to about 65%, the particle (glass particles of 300 μm)

mobility decreased. When the humidity was increased above 65%, the particles became immobile. Introducing interparticle forces by increasing humidity or using nonvolatile liquid layers on the particles, it is possible to change the fluidization behavior of particles [Gel84].

In the translational relative humidity region around the critical relative humidity incremental changes in processing characteristics can occur and can lead to a loss of process control. In this research, the critical humidity range and its effect on the coating efficiency of primary particles with secondary particles was investigated as one of the critical parameters in synthesis of composite particles.

Surface Roughness

Adhesion equations can only be used for smooth surfaces. However, in reality, molecularly smooth particles exist very seldom, especially in industrial conditions. Solid surfaces, irrespective of their method of formation, generally contain surface irregularities. The adhesion observed between hard solids when placed in contact is very small. This may be due either to surface films or to surface roughness. However, experiments between hard elastic solids such as TiC, sapphire and diamond cleaned in the vacuum show that low adhesion is due, not to surface films, but surface roughness [Gan74].

Adhesion of a particle to a substrate surface involves the following essential steps.

At first, particle and substrate come into contact at one point by a contact area of atomic dimensions.

Then, by long-range attraction forces between the two, the particle generally is subject to a moment of force so that several contacts are formed.

Finally, by the interaction forces, the contact area at these contacts increases until the attractive forces and the forces resisting the further deformation at the interface are in equilibrium. An adhesive area of finite size is formed between the adherents [Kru67].

When two nominally flat surfaces are placed in contact, surface roughness causes contact to occur at discrete points. The sum of the areas of all the contact points constitutes the real area of contact, and for most materials at normal loads, this will be only a small fraction of the area that would be in contact if the surfaces were perfectly smooth. In general, this real area of contact must be minimized to minimize adhesion, friction and wear [Bhu95].

The study of the influence of surface roughness on adhesion has a rather short history. Wenzel [Wen36] in 1936 suggested that the introduction of surface roughness at a contact would increase the surface area in contact and hence increase the adhesion. The Wenzel coefficient, that is, the

ratio of real area to apparent area, is still often but perhaps ill used as a predictive tool. The supposition is that the adherent fully wets the substrate [Bri94].

The asperities on the surface reduce the area of intimate contact. Even more important factor is introduced by the dispersion of asperity heights since a few high asperities may be very effective in pushing the adhering surfaces apart. Especially high modulus make the adhesion much more sensitive to surface roughness [Tab77].

The first systematic study was done by Fuller and Tabor [Tab75] to measure the effect of surface roughness on adhesion by using rubber spheres and a perspex surface roughened to various degrees. They obtained a modified adhesion parameter called θ given by

$$\theta = \frac{E\sigma^{3/2}\beta^{1/2}}{\beta\Delta\gamma}. \qquad (2.11)$$

The denominator is a measure of the adhesive force experienced by a sphere of radius β while the numerator is a measure of the elastic force needed to push a sphere of radius β to a depth σ into an elastic solid of modulus E. The adhesion parameter represents the statistical average of a competition between the compressive forces exerted by the higher asperities which are trying to separate the surfaces and the adhesive forces between the lower asperities which are trying to hold the surfaces together. When the adhesion

parameter is small, the adhesive factor dominates. When the surface roughness and hence the adhesion parameter increases adhesion falls to a very small value. The theory predicts that the adhesion is determined by the value of one parameter, the ratio between the dispersion of asperity heights which was characterized by "center line average" (cla) as measured on a profilometer. The results for roughened surfaces are shown in figure 2-13. The vertical axis is the pull-off force expressed as a fraction of the pull-off force for the same rubber specimen in contact with a smooth surface. The horizontal axis is the center line average of the roughness.

Figure 2-13 shows that a roughness of 1 μm reduces the adhesion to a very small fraction of its value for smooth surfaces. Increasing the modulus of elasticity by a factor of 10 noticeably increases the rate at which the adhesion falls with increasing roughness.

A more quantitative calculation was done by Iida et.al.[Iid93] by using a smooth glass particle and glass substrate roughened to three different roughness values ranging from 50 nm to 0.4 μm. Roughness was characterized by an STM using center line average values and the force of adhesion was measured by the impact separation method [Iid93]. The method measures average adhesive force for 50% of particles remained on the substrate after separation. Adhesion force

was observed to drop by a factor of 10 with increasing centerline average roughness.

Schaefer et al. [Sch94] have investigated the reason of low adhesion force experimentally observed compared to the calculated adhesion force from JKR model. The forces were measured by AFM and the roughness was characterized by estimating a mean radius of curvature from AFM line scans. It was concluded that the adhesion force is reduced by a factor of 13 to 16 with an increase in surface roughness.

It is crucial to accurately calculate the adhesion force change within very small deviations from an ideal smooth surface for many industrial needs such as to control particle deposition especially on wafers. There is no experimental observation available in the literature for the adhesion force change within a few nanometers roughness increase. The range of roughness is either on the micron-scale or tens of nanometers. The reason for the lack of experimental data is due to experimental and theoretical difficulties. The experimental difficulty is obtaining rough surfaces having regular and reproducible profiles for nano-size regimes. The theoretical difficulty arises from the interpretation or characterization of roughness and definition of a correct geometric model representing the experimentally measured roughness parameters. Also the horizontal feature of roughness namely, wavelength is missing and the calculations

are based on the value of one parameter usually, the radius of asperity or roughness peak as was the case in Rumpf's approach [Rum78] or the ratio between the dispersion surface asperity heights which were characterized by "center line average" (c.l.a.) from profilometer or STM measurements. However, at least two functions are necessary to sensibly describe the topography of a surface [Bri92]. Characterization of surface roughness is important for predicting and understanding the adhesion of particles to surfaces. In that regard, one of the most known approach to adhesion of rough solids was suggested by Rumpf [Rum78]. The approach is based on the model shown in figure 2-14, where roughness is ideally represented by an asperity in the form of a semi-sphere of radius *r* with its center placed on the surface. Two types of interaction of a sphere with radius *R* are taken into account namely, with a rough peak and with a flat surface. The first interaction is the "contact" one, because interacting solids are placed in the contact position, while the second interaction is a "non-contact" one, because solids are separated by a gap larger than intermolecular distance. Using Derjaguin's approximation [Der75] for both interactions, Rumpf [Rum78] obtained the following formula to calculate van der Waals adhesion force

$$F_{ad} = \frac{h\varpi}{8\pi}\left(\frac{r}{Z^2} + \frac{R}{(r+Z)^2}\right) \qquad (2.12)$$

where Z is the intermolecular separation distance between two bodies, and r is the radius of the rough peak.

Xie [Xie97] developed a similar approach assuming the asperity as a small particle in between two large particles. The distance between two large spheres is increased to 2Z+d as shown in figure 2-15. The radius of roughness peak in figure 2-14 is expressed by the radius of particle in figure 2-15.

The total vdW force now consists of the force between the two large spheres $F'=AD/12(2Z+d)$ plus the force between the smaller particle and two spheres which is: $F''=A(D_1+D_2)/12Z^2$. The total force of this sandwich like contacting system is

$$F_t = \frac{AD}{12(2Z+d')} + \frac{A(D_1+D_2)}{12Z^2} \tag{2.13}$$

where $D=R_1R_2/R_1+R_2$ and $D_1=d'R_1/d'+R_1$ and $D_2=d'R_2/d'+R_2$.

According to the model, the interaction between the two parent particle decreases as the size of the smaller particle increases; the interaction between the smaller particle and the parent particle dominates the total interaction when the smaller particle is larger than 0.1 μm. The total force was observed to be the same as the force between the parent spheres when the asperities are smaller than 0.01 μm. It was concluded that if the radii of surface asperities are larger than 0.1 μm, the diameter in the equations for calculating van der Waals forces should be replaced by the size of the surface

asperities; if the radii are smaller than 0.01 μm, the particles could be treated as smooth.

In this research, an accurate quantification of adhesion force as a function of very small roughness changes within a few nanometers range was investigated by using the Atomic Force Microscope. Adhesive force calculations were obtained on controlled rough surfaces of Ti-coated silicon wafers with sphere and tip interactions. A new theoretical approach to calculate adhesion force as a function of roughness has been developed considering both vertical and horizontal features of roughness using RMS (root mean square) roughness and λ as surface roughness parameters.

The Effect of Contact Deformation

The spreading or contracting of one liquid surface over another or over a solid surface to reach an equilibrium state is dominated by the minimization of surface energy. For example, when a liquid drop is brought into contact with a solid surface its final contact size at equilibrium may be predicted from surface energy considerations. On the other hand when a contact is formed between two smooth solid surfaces, the equilibrium largely depends upon the distribution of elastic forces in the contacting bodies.

The contact between two smooth elastic bodies was investigated by Hertz (1896) who demonstrated that both the size and shape of the zone of contact followed from the elastic deformation of the bodies. For two spheres of radius R_1 and R_2 pressed together under a load P the radius "a" of the circle of contact is given by;

$$a^3 = \frac{3}{4}\pi(k_1 + k_2)\frac{R_1 R_2}{R_1 + R_2}P \tag{2.14}$$

where $k_1 = \frac{1-\nu_1^2}{\pi E_1}$, $k_2 = \frac{1-\nu_2^2}{\pi E_2}$ and ν is the Poisson ratio, E is the modulus of elasticity. Hertz used an optical microscope to measure the contact between glass spheres and so verified his theory experimentally.

However, some experimental contradictions to Hertz theory have been reported. Roberts (1968) using smooth rubber spheres and Kendall (1969) using glass spheres noted that at low loads contact areas between these bodies were considerably larger than those predicted by Hertz [Joh71]. Strong adhesion was observed if the surfaces were clean and dry.

These observations strongly suggested that attractive surface forces were operating between the solids and although these 'additional' contact forces were of little significance at high loads they became increasingly important as the load was reduced toward zero.

The Hertz equation, modified to take into account the surface energy effect is [joh71]

$$a^3 = \frac{R}{K}\left(P + 3\gamma\pi R + \sqrt{6\gamma\pi RP + (3\gamma\pi R)^2}\right) \qquad (2.15)$$

where $K = \frac{4}{3\pi(k_1 + k_2)}$

When γ=0 the equation reverts to the simple Hertz equation. At zero applied load the contact area is finite and given by

$$a^3 = R(6\gamma\pi R)/K \ . \qquad (2.16)$$

When the applied load is made negative, the contact radius decreases. For a real solution to be obtained to equation (2.14); $6\gamma\pi RP \leq (3\gamma\pi R)^2$ and $P \leq 3/2\gamma\pi R$ have to be satisfied.

Separation of the spheres will just occur at $P=(3/2)\gamma\pi R$ which is not dependent on the elastic modulus. The modified Hertz theory (JKR), equation (2.15) appears to account for the observed contact results between smooth surfaces of rubber and gelatine. It predicts both a contact radius greater than the calculated Hertz radius at light loads as shown in figure 2-16 and also the negative load (adhesion force) needed to separate bodies.

An alternative approach for calculating the contact radius between a particle and a substrate was proposed by Derjaguin, Muller and Toporov (DMT model) [Der75]. Assuming

that the shape of the contact region would be Hertzian, DMT model predicts that half of the interactions occurs outside of the contact zone. This is in contrast with the JKR model, which assumes that all interactions occur within the radius of contact. However, there is only a coefficient difference between JKR and DMT theories in calculating adhesion force where adhesion force predicted by DMT model is 4/3 of those predicted by JKR model.

Following a somewhat heated debate in the literature, Muller et al. [Mul80, Mul83] showed that discrepancy between the two models arises from the differing assumptions regarding the occurrence of a non-zero potential outside the contact radius. Moreover, they showed that the JKR and DMT model each have a region of validity, which can be defined in terms of a dimensionless parameter μ, such that;

$$\mu = \frac{32}{3\pi}\left[\frac{2RW_A}{\pi E^* z^3}\right]^{1/3} \tag{2.17}$$

where $$\frac{1}{E^*} = \frac{(1-\nu_1^2)}{E_1} + \frac{(1-\nu_2^2)}{E_2}$$

If $\mu>1$, corresponding to large particles, high surface energy materials, and low elastic moduli, the adhesion-induced deformations are described by the JKR theory. Conversely, if $\mu<1$, DMT model is valid.

Finally Maugis and Pollock (MP model) generalized the JKR model to include plastic deformations [Mau84]. They found that in the case of plastic deformations, the contact radius 'a' is related to the particle radius R and any externally applied load P by

$$P + 2\pi w_a R = \pi \rho^2 H \qquad (2.18)$$

where w_a is the work of adhesion and H is hardness of the material.

The effects of deformation on adhesion forces are often treated in the literature using energy methods mentioned above. However, Dahneke [Dah72], Cotaar and Rietema [Cot85], Tsai et al. [Tsa91] and Xie [Xie97], used Hamaker theory to study the effects of particle deformation on adhesion forces by calculating the surface energy from intermolecular interactions over two contacting bodies, which has the advantage that it is independent of the nature of the deformation.

When two spheres come into contact, flattening of their tips can occur in several ways depending on their relative hardness. The deformation is idealized as shown in figure 2-17. As a first order approximation, the distance between the two deformed bodies is taken as a constant, Z_0, which is assumed to be 4 Å. Xie calculated the total attractive energy by van der Waals equation over the two deformed particles. He

found that the van der Waals force due to deformation is increased by a factor of $(s/\pi Dz_0)$, where s is the area of deformation in the contacting system ad D is the equivalent diameter of the two particles [Xie97].

Tsai et al. [Tsa91] have developed an equilibrium adhesion parameter ($\prod$) from the elastic energy and Hamaker approach and defined the adhesion parameter as a function of deformation parameter, α/z_0. The deformation parameter represents a factor that must be multiplied to F_{ad} (equation 2.1). Hence for large deformations, $\alpha/z>>1$, the adhesion force is much greater than that predicted by equation (2.1) especially when dealing with soft systems. The effect of elastic flattening on adhesion force was shown in figure 2-18, where K is the deformation parameter. In soft systems when $\prod>>1$, elastic flattening becomes substantial. As an example, when $\prod=100$, the attractive force at static equilibrium is 52 times higher than that without considering elastic flattening. For particle diameters ranging from 0.01 to 100 mm, the $\prod$ ranges from 0.01 to 5 for metals and oxides, and from 5 to 200 for polymers [Tsa91].

The rapid developments in the atomic force microscope with a new generation of cantilever tips have allowed detection of minute deflection of the cantilever. The force between an AFM tip and a surface can be measured with a

resolution of better than 0.1 nN [Duc91]. The development of these new techniques allows quantitative studies of the relevant microscopic contact forces acting on objects near a flat surface which constitutes a part of this research.

Impact of Particles

The impact of particles with surfaces occurs in a variety of situations such as filtration, surface contamination, spray coating, including MAIC process used in this research.

When spherical particles of most engineering materials with diameters well above 100 μm collide with each other or with a surface at very low velocities, the collisions are almost perfectly elastic and the ratio of the final normal velocity to the initial normal velocity tends to approach a value near unity. As the initial velocity is increased, the ratio, often called the coefficient of restitution, decreases usually monotonically and significantly [Bra92].

A schematic diagram of the particle bounce process treated as a simple energy balance is shown in figure 2-19 [Wal90]. An energy balance for the impact is $K_i+E_i-K_L=K_r+E_r$ and rebound occurs for $K_e>E_r$, where K_i and K_r are the kinetic energy for the incoming and rebounding particle, E_i and E_r are the potential energy of interaction with the surface for the

incoming and rebounding particle, and K_L is the energy loss during the impact [Wal90].

Bitter [Bit63] has determined the limiting velocity V_y, above which plastic deformation begins to occur as:

$$V_y=(2\pi/3K)^2(2/5\rho)^{1/2}Y^{5/2} \qquad (2.19)$$

where ρ is the density of the particle, Y is the Y is the yield strength and K is the same mechanical constant in equation (2.15). The limiting velocity is determined by the bulk material properties and is independent of particle size. As an example, the bulk properties of polystyrene are known to be $K=2.75\times10^{-10}$ m^2/N, $\rho=1.05\times10^3$ kg/m^3, and $Y=4.8\times10^7$ N/m^2. Plastic damage would be expected to occur for impact velocities as small as 0.06 m/sec [Wal90].

The critical velocities for particles to be captured by the surface were determined by extrapolation of the energy balance equation to zero rebound velocity [Tsa90]. There are three important phenomena that are inherent in the impaction process and are major energy loss mechanisms. These are the breaking of the contact surface, bulk deformation and surface roughness. If these mechanisms were absent, there would have been no energy loss. Particles would then always rebound with the same incident velocity as that of the incident particle. Figure 2-20 shows relative percentage of three different energy loss mechanisms [Tsa90]. The local plastic deformation

energy loss is most dominant in the case where the surface is rough. In the case where the surface is perfectly smooth, the sole energy loss is due to breaking of the contact surface. Energy loss due to bulk plastic deformation prevails as soon as it occurs. Critical velocities for rebound increased with decreasing particle size, ranging from 1.1 m/sec for 7 μm to 3.6 m/sec for 2.5 μm for molybdenum particles [Wal90]. Figure 2-21 shows the critical velocities which particles rebound upon collision between ammonium fluorescein particles and mica targets [Wal90]. Dahneke's theoretical calculation of critical speed is shown in figure 2-22 for different surface roughness values [Dah75].

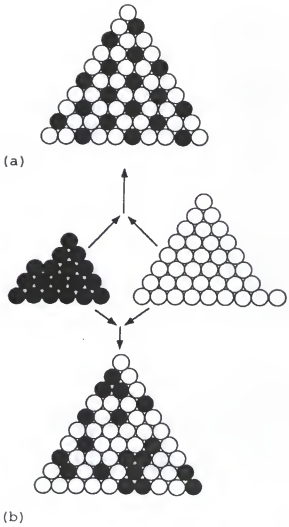

Figure 2-1. Comparison of a) ordered and b) random mixture from two different particles.

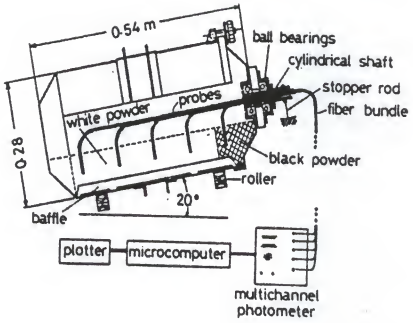

Figure 2-2. Schematic of rocking type mixer.

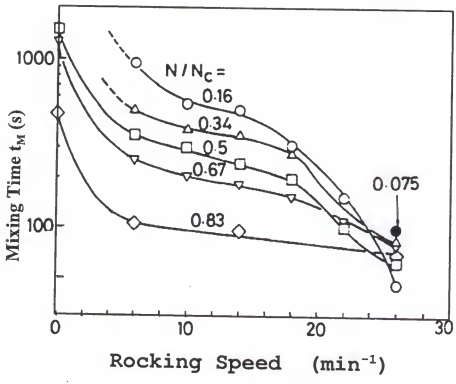

Figure 2-3. Effect of rocking speed on mixing time.

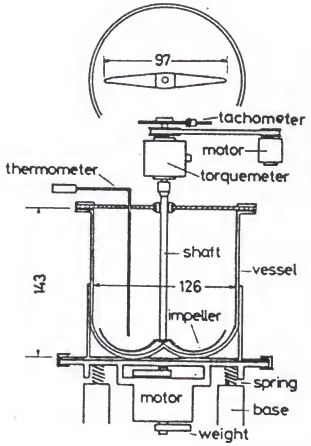

Figure 2-4. Schematic of high speed stirred mixer.

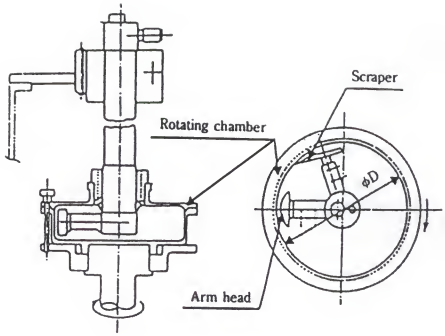

Figure 2-5. Schematic of mechanofusion system.

● System flow-chart

1. O.M.dizer
   (formation of "ordered mixture".)
2. Weighing machine (Feeder)
3. Hybridizer
   (embedding/filming processes)
4. Collector
5. Control & Operation Panel

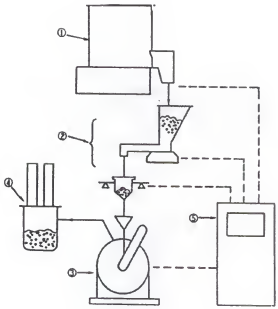

Figure 2-6. Schematic of hybridization system.

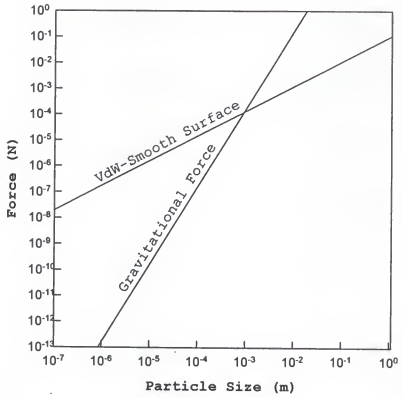

Figure 2-7. Comparison of van der Waals and gravitational forces.

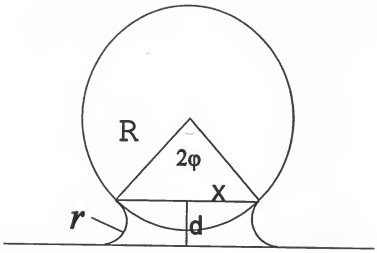

Figure 2-8. Liquid bridge joining particle to surface.

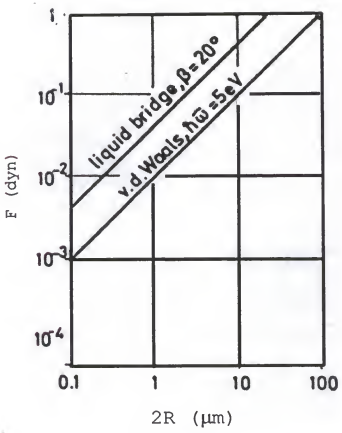

Figure 2-9. Comparison of van der Waals and capillary forces.

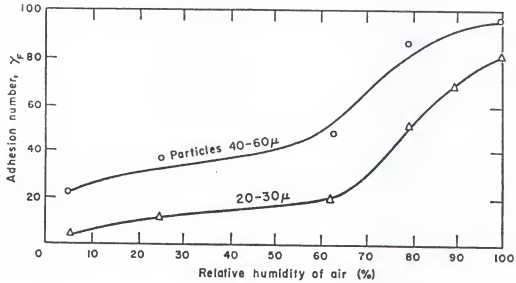

Figure 2-10. The influence of humidity on adhesion.

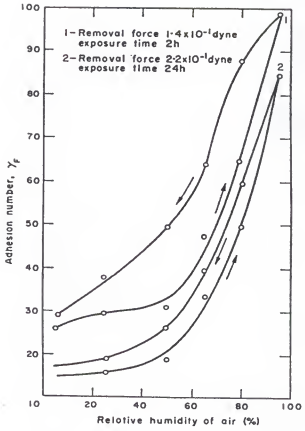

Figure 2-11. Hysteresis of adhesion of particles as a function of humidity.

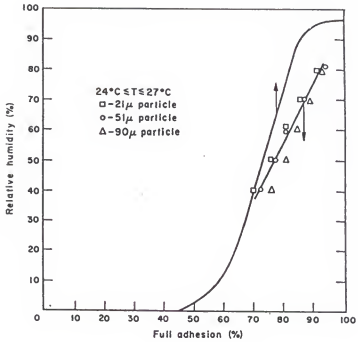

Figure 2-12. Adhesion variation as a function of humidity for quartz particles on pyrex flat.

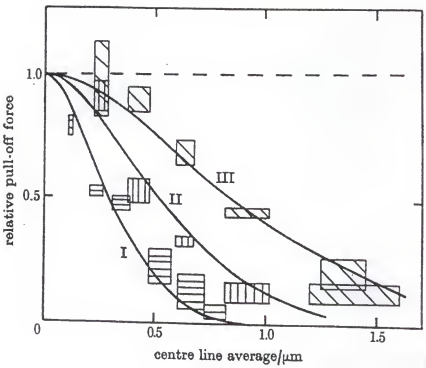

Figure 2-13. Relative pull-off force for smooth rubber spheres in contact with a flat Perspex surface as a function of the roughness of the perspex. Effects of modulus, E, of the rubber: curve I, 2.4×10^6 N/m^2; curve II, 6.8×10^5 N/m^2; curve III, 2.2×10^5 N/m^2.

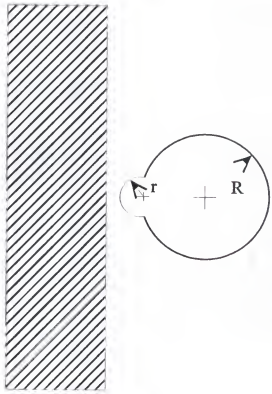

Figure 2-14. Rumpf's model of particle-surface adhesion for rough surface.

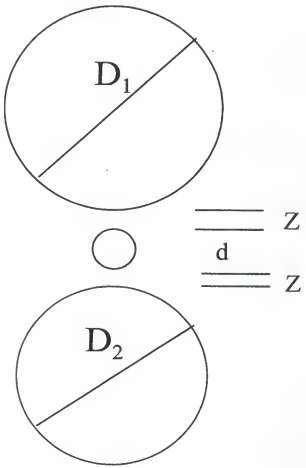

Figure 2-15. Xie's model for definition of roughness.

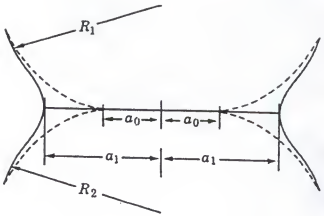

Figure 2-16. Contact region between two particles (R_1 and R_2) according to Hertz (dashed line) and JKR theories. The radius of contact is a_0 and a_1 in case of Hertz and JKR theories respectively.

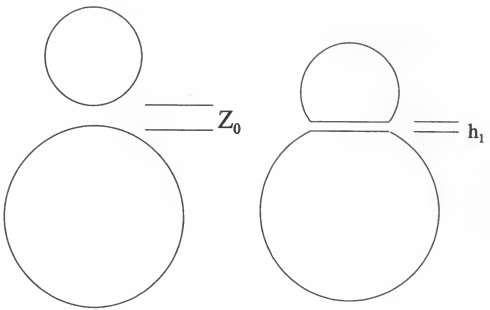

Figure 2-17. The deformation at the contact region showing flattening of tips when two spheres come into contact.

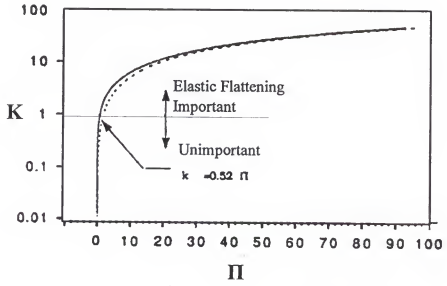

Figure 2-18. Equilibrium deformation parameter K versus adhesion parameter Π showing the region where elastic flattening is important.

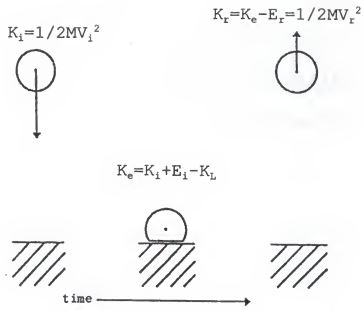

Figure 2-19. A diagram of the particle bounce process as a simple energy balance for impacts showing the incoming particle approaching the surface, at full compression and at rebounding.

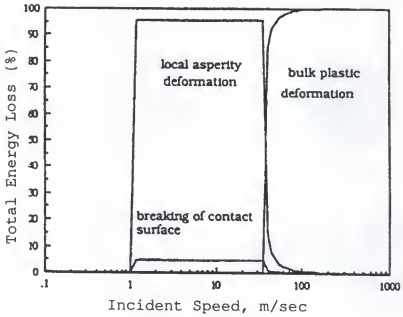

Figure 2-20. Percent of the total energy loss due to different mechanisms for 1.27 μm PSL on quartz surface for r_{asp}=0.01 μm.

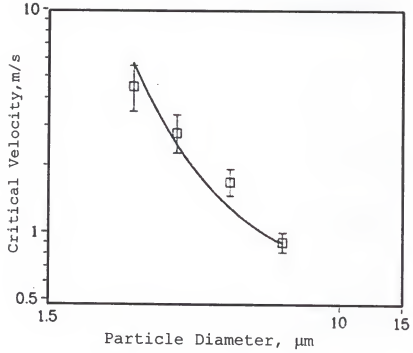

Figure 2-21. Critical velocity for rebound versus particle size for mica target material with ammonium fluorescein spheres.

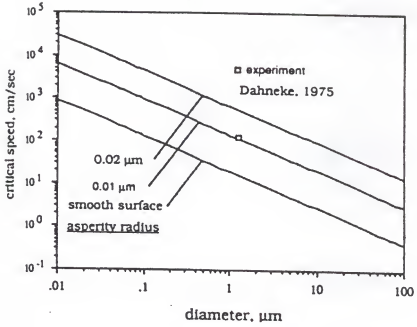

Figure 2-22. Comparison of the critical speed for rebound at different roughness levels as a function of particle size for PSL on quartz.

CHAPTER 3
EXPERIMENTAL APPROACH

Introduction

An advanced technology to manufacture composite particles with a uniform thin or thick coating layer or controlled shape and composition, depends on the fundamental understanding of the adhesion between particles and surfaces. Therefore this research focuses on both synthesis and characterization of composite particles as well as adhesion behavior of composite particles under various conditions such as, humidity, surface roughness, external loading.

Magnetically assisted impaction coating (MAIC) process has been used to synthesize composite powders. A detailed description of the MAIC process and the mechanism of composite formation are presented. The influence of processing parameters such as processing time, particle loading, applied current and frequency of the field, the use of low pressures are studied. The role of humidity, particle size, external pressures, surface roughness and particle velocity which are the major parameters affecting composite formation as well as

the adhesion of particles are addressed.

Scanning electron microscope (SEM) JEOL JSM 6400 operating at 15 kV and a working distance of 15 mm was used to record morphology of the composite particles. Atomic Force Microscope (AFM) Nanoscope III, (Digital Instruments Inc., Santa Barbara, CA.) was used to quantify adhesion forces between particles and surface. A CCD camera with 30 frames/second recording speed and a High Speed Camera (Kodak Exta Pro intensified image system) with a 1000 frames/second recording speed were used to observe the in situ movement of particles.

Description of MAIC System

Overall, the MAIC system (Aveka Inc. Woodbury, MN55125) consists of electromagnets that create an alternating magnetic field and a cylindrical glass chamber containing magnetic, primary and secondary particles as shown in figure 3-1. Magnetic particles are accelerated upon application of an AC current with a varying frequency (45-100 Hz) and voltage (30-70 V).

The powder mixture is fluidized by means of collisions initiated by magnetic particles which have haphazard, random movements. As a result a collision environment is formed in the chamber. The agglomerates are broken and free secondary

particles are created. The size similarity between primary and magnetic particles promotes a strong impaction between them. Thus, various types of forces mainly compression and shear are exerted on the agglomerates which is the main advantage of the MAIC system. The agglomerate free secondary particles in turn adhere to large primary particle surfaces forming a coating layer.

Magnetic particles are $SrFe_{12}O_{14}$ based magnets having irregular geometry as shown in figure 3-2. They are Teflon coated to prevent contamination. Three different sizes of magnetic particles were used as 160, 840 and 2000 μm. In Most of the experiments larger sizes were used.

A weak alternating magnetic field (~100 Gauss) is generated across the chamber by applying an AC field to the electromagnets. Figure 3-3 shows magnetization as a function of the applied magnetic field (B-H hysteresis loop) obtained from a SQUID magnetometer. The field applies a torque on the irregularly shaped magnetic particles and accelerates them in a non-periodic fashion. The magnetic particles are characterized by a high coercivity (~4000 Gauss) so that they do not reverse their polarity in the weak electromagnetic field. After the formation of the coating, the magnetic particles are separated from the composite particles by standard magnetic separation methods.

The MAIC process can be controlled by controlling the frequency, intensity or potential difference of the electric field around the magnets.

Materials Used

In the majority of experiments Polymethylmethacrylate (PMMA) having smooth surfaces and nearly spherical shape were used as primary particles. Glass beads (soda-lime glass $70SiO_2$,$10CaO$,$15Na_2O$) of 200 μm and Al_2O_3 (AA18 Sumitomo) of 20 μm in size were also used as primary particles in some of the experiments. As far the secondary particles are concerned, Al_2O_3 was used because of its commercial availability at various sub-micron sizes. Table 3-1 shows a list of the starting materials including their manufacturer.

Table 3.1. Particles used in MAIC experiments

Particle Type	Powder	Average Size (μm)	Manufacturer
Primary	PMMA	200	Polysciences Inc.
Primary	Glass Beads	100	ER-Advanced Ceramics
Secondary	Al_2O_3	0.05	Buehler
Secondary	Al_2O_3 (AKP-50)	0.2	Sumitomo
Secondary	Al_2O_3 (AKP-30)	0.4	Sumitomo
Secondary	Al_2O_3	1	Buehler
Magnetic	$SrFe_{12}O_{14}$	160-2000	Aveka Inc.

Particle Loading

Primary and secondary particles were placed in a 50 ml glass container without any premixing. The ratio was adjusted so that a mono-layer surface coverage is obtained around the primary particles. The characterization of surfaces was done by SEM using image analysis techniques i.e. line analysis. The total amount of primary and secondary particles was kept constant around 2 grams for each loading in proportional to the size of glass chamber.

A series of MAIC experiments were conducted at different proportions of magnetic particles (magnets) and powder ratios to determine the optimum ratio.

Particle Size

The effect of particle size on the composite formation was investigated by coating alumina secondary particles of various sizes on PMMA (200μm) and alumina (20 μm) primary particles. Primary particles compared to the size of secondary particle can be assumed as flat surfaces. The drawing in figure 3-4 shows an enlarged real size view of a 1 μm particle vs 20 μm and 200 μm particle. Therefore the interaction between primary and secondary particles is

particle-flat rather than particle-particle interaction. Due to that fact, the size change in primary particles have no significant effect in terms of adhesion forces. Thus, the major size parameter in composite particle formation as far as the adhesive forces is concerned is the size of secondary particles.

Secondary particle sizes in the range of 0.05 μm to 1 μm was investigated. Since 1 μm size range yielded very poor surface coverage, larger sizes were not investigated. The surface coverage around the primary particles were calculated from SEM pictures using standard image analysis techniques.

The difference in the adhesive forces due to change in the size of the particle was also studied with an AFM using 10 μm glass spheres and the AFM tip which is nearly 50-100 nm in size. Sphere and tip are interacted at which short range interatomic forces determines the strength of adhesion with silicon wafers of different roughness.

Processing Time

The effect of processing time was investigated by conducting MAIC experiments at five different durations as 1, 3, 5, 7 and 10 min on PMMA/Al_2O_3 primary-secondary particle combinations. In addition nano-size range was studied by

coating silver nano-particles of 30-50 nm on Al_2O_3 primaries at 1, 3 and 5 min intervals. The surface coverage after each run was analyzed from SEM images.

Humidity Studies

The effect of humidity on the composite particle formation was investigated in two parts. The first part is the effect of humidity on composite particle formation in MAIC process. The second part is the adhesion force measurements under various humidity levels using AFM.

In the first part, the efficiency of coating as a function of humidity was analyzed by inserting MAIC unit inside a humidity chamber as shown in figure 3-5. The humidity of the chamber was controlled by a hygrometer with +/-2-5% sensitivity and the range was varied from 5% to 85% relative humidity (RH). The humidity of normal air in laboratory conditions is around 55% RH. Samples were kept in the chamber for a couple hours before running the experiments for conditioning and equilibrium purposes.

In the second part, the surface forces were measured under varying humidity levels by putting AFM piezoelectric unit into humidity chamber

A relatively smooth glass sphere of 10 μm in radius and 0.2 nm in roughness was attached to the AFM cantilever tip

with a resin epoxy type glue. The effect of glue on adhesion strength is negligible due to very small thickness (<2nm). The configuration of particle attached to AFM cantilever is shown in figure 3-6A. The glass sphere was interacted with alumina and silver flat surfaces having 0.2 nm and 1.2 nm surface roughness respectively. Both AFM measurements and MAIC experimental conditions are particle-flat interactions.

The AFM cantilever has dimensions of 200 μm long, 36 μm wide and 0.6 μm thick. The spring constant is 0.0064 N/m. A Si_3N_4 tip is provided at the end of cantilever The top radius of the tip is estimated to be nearly 50 nm as shown in figure 3-6B from the SEM picture.

Surface roughness also alters the capillary forces. The effect was studied by using controlled rough surfaces of Ti deposited Si wafers (Motorola Inc.).

The results from the two parts of the humidity study were compared and correlated.

Forces acting between particles and surfaces were measured using Atomic Force Microscope (Nanoscope III, Digital Instruments Inc., Santa Barbara, CA.) as shown in figure 3-7. The information about the local elastic, plastic or capillary forces were obtained from force vs. distance curves as shown in figure 3-8. A force vs. distance curve is a plot of the deflection of the AFM cantilever tip in the z direction as a

function of the extension of the piezoelectric scanner, measured using a position sensitive photodetector. The force acting on the probe is determined from the deflection of the cantilever. The sensitivity of the measurement of the probe deflection is 0.3 nm, and thus, that for the applied force is approximately 20 pN. When the AFM probe or cantilever approaches the sample, a sudden attractive force is exerted on the probe. As the sample stage moves closer, the force changes from attractive to repulsive. In the repulsive region, the distance between the probe and the sample is very small and the probe is considered to be in contact with the sample surface. When the sample, which in contact with the probe, moves further, the deflection of probe increases linearly as a function of sample displacement. Retracting the probe results a decrease in the repulsive force. The retracting curve is often different because a monolayer or a few monolayers of water are present depending on the relative humidity conditions. This water layer exerts a capillary force. As the probe pulls away from the surface, the water holds the tip in contact with the surface, bending the cantilever strongly towards the surface. At some point, depending on the thickness of the water layer, the probe retracts enough that the tip springs free. This is known as the snap-back point. As the probe continues to retract beyond that point, the cantilever remains undeflected. The

snap-back point is the point at which the probe overcomes any type of dominant adhesion force between particle and surface.

The Effect of Loading Force

The dependence of adhesion on loading force was studied using the AFM. In the past, this has been done in a statistical way by measuring the fraction of particles removed as a function of the lift off force. The force of removal has been measured using techniques such as electrostatic detachment and centrifugation [Zim80].

Two types of materials, an easily deformable, soft PMMA and an elastic, hard Al_2O_3 were used as substrates to observe the change in the adhesion forces as a function of loading force. The pressure applied by the AFM Si_3N_4 tip was in the range 50-1400 nN.

The AFM measurements were correlated to MAIC experiments in which, PMMA and Al_2O_3 primary particles were coated by AKP-50 Al_2O_3 secondaries. The strength of coating was tested by putting the samples into an ultrasonication bath after the coating was completed. Ultrasonication is a technique that is qualitatively used to test the relative strength of adhesion. It is advantageous in a sense that it gives information about overall adhesion strength of the coating rather than individual particles as in the case of AFM. Both techniques

are complementary to each other and were utilized in this study.

Surface Roughness

The change in adhesion force as a function of surface roughness was measured experimentally using the AFM. Experiments were conducted in a chamber with controlled humidity of nearly 20% to shield capillary force effects.

Part of the experiments were conducted by interacting a flat surface with a smooth glass sphere of 10 μm in radius. The sphere was attached to AFM cantilever tip under an optical microscope with a thermoplastic type resin epoxy glue. Other series of experiments were made by bringing pyramidal AFM Si_3N_4 tipin contact to a flat surface. The experimental configuration is shown in figure 3-9.

Titanium deposited Si-wafers (Motorola Inc.) were used as a flat surface because of their availability at various roughness values. Surface chemistry of the samples were measured by Auger Electron Spectroscopy. Figure 3-10 shows the Auger spectrum for 3 min sputtering time. Titanium and oxygen was detected at the topmost layer. Before starting adhesion measurements, samples were cleaned by rinsing with ethanol, methanol and de-ionized water and dried by blowing dry gas, tetrafluoroethane.

The AFM topographic images and surface roughness profiles for various samples of coated silicon wafer are shown in figures 3-11,3-12. In these figures, the peaks look like approximately semi-spherical; however, it is a wrong impression related to the non-equal horizontal and vertical scales. Two different types of roughness profiles were observed. Roughness associated with long wavelength fluctuations is called RMS_1 and one associated with shorter wavelength is called RMS_2. For relatively flat samples, sample #1 and #2, there is no long range wavelength profile as can be seen in the figures 3-11 a,b and therefore only an RMS_2 value was used in adhesion force calculations. On the other hand for samples #3 and #4, a fluctuation of a long wavelength was observed in addition to short nano-scale wavelengths as can be seen in Figures 3-11 c, d. Surface topographic images from AFM scans of sample #2 and 4 are shown in figure 3-12. Experimental RMS and wave length parameters found from the images, are given in table 3-2. Values of RMS were calculated with standard software and values of λ were found as average value for various sections. The radii for peak roughness were calculated with equations suggested below using experimental values of RMS and λ.

Table 3-2. Experimental values of the roughness profile parameters, λ and RMS, for various samples.

Sample	RMS_1 (nm)	RMS_2 (nm)	λ_1 (nm)	λ_2 (nm)
1*	0	0.17	-	250
2	0	1.64	-	249
3	4.3	1.64	1180	237
4	10.5	1.64	1046	260

*Sample 1 is non-coated silicon wafer.

Particle Movement and Velocity

The movement of magnetic and primary particles was studied using a high speed (1000 frames/second) Kodak Exta Pro intensified image system. The behavior of magnetic particles (1500-2000 μm) was observed in the presence of alumina primaries of 800 μm in diameter as a function of varying frequency and current conditions. The velocity of magnetic particles was recorded. The movement of secondary particles cannot be observed due to their small size which requires specialized lenses. The surface coverage obtained at different frequencies were plotted as a function of velocity.

Collision Frequency

MAIC process can be controlled by varying the frequency of collisions or adjusting the processing time. Collision frequency depends on the number, size and velocity of the constituent particles as well as the frequency of magnetic field or current.

The change in the surface coverage of alumina primary particles of 20 μm in size as a function of magnetic particle collision frequency was studied. AKP-50 alumina was used as secondary particles.

The collision frequency of magnetic particles was calculated according to the equation:

$$f=N_1.N_2.\pi.\ (R_1+R_2)^2.V \qquad (3.1)$$

where N1 and N2 are the number, R1 and R2 are the radius of magnetic and primary particles respectively, and V is the average velocity of particles. The frequency of collisions was changed by varying the size of magnetic particles for the same optimum loading of the chamber (a total of 2 gr powder loading). The surface coverage was determined from SEM pictures.

Low Pressure or Vacuum Effects

An evacuation device was added to the original apparatus enabling it to reduce pressure down to 200 mTorr. Two sets of experiments, one is at 200 mTorr and the other at 700 mTorr were conducted to observe the role of low pressures in composite formation.

The glass processing chamber containing PMMA and AKP-50 powder mixture and magnetic media, was first evacuated. An argon gas flow was switched on through chamber to adjust the pressure level. After reaching to a stable low pressure regime, MAIC process run for 5 min.

The strength of bonding or adhesion between the low pressure and normal atmospheric pressure treated samples were compared using an ultrasonication device operating around 20 kHz frequency. The composite powder mixture was put in a DI water filled glass bottle. The ultrasonicated powder mixture was passed through a series of filter assembly to remove water and then dried using very low temperatures.

The SEM images of the samples was analyzed to calculate the surface coverage for vacuum treated, normal pressure treated or ultrasonicated samples.

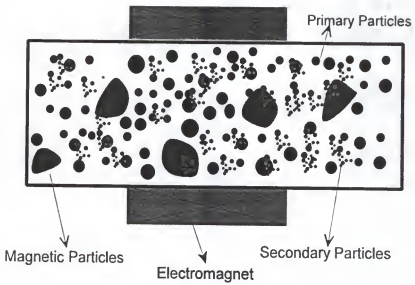

Figure 3-1. Schematic diagram of the magnetically assisted impaction coating (MAIC) system.

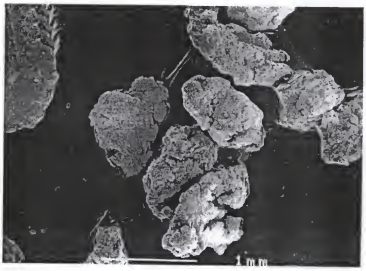

Figure 3-2. SEM image of magnetic particles.

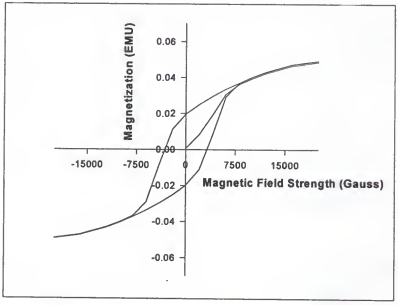

Figure 3-3. Magnetization versus applied magnetic field for magnetic particles used in the MAIC system.

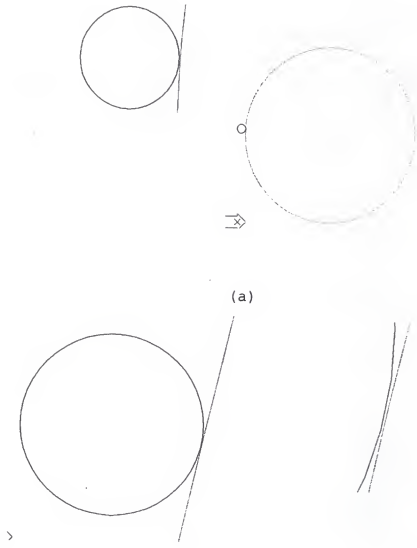

Figure 3-4. Schematic comparison (scaled in size) of a) 20 μm and b) 200 μm primary particle with 1 μm secondary particles.

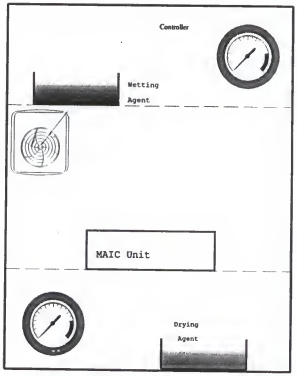

Figure 3-5. Humidity chamber used to adjust the relative humidity during the experiment.

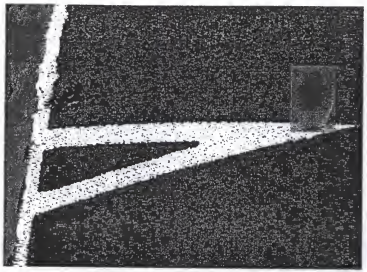

(a)

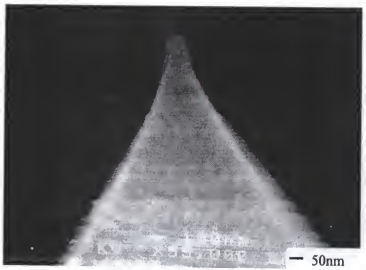

(b)

Figure 3-6. a) SEM picture of an AFM cantilever and a particle attached. b) The magnified SEM image showing the AFM tip.

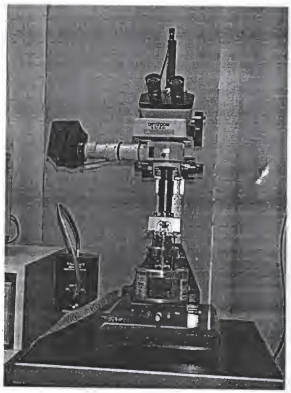

Figure 3-7. Nanoscope III Atomic Force microscope.

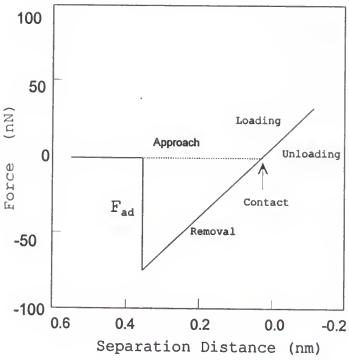

Figure 3-8. Force vs distance plot.

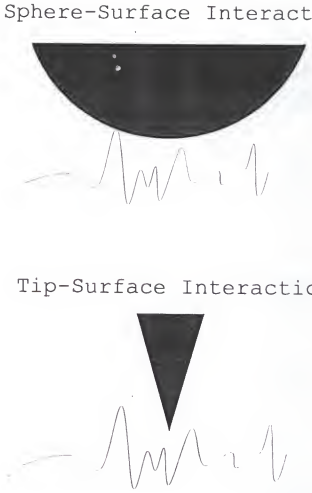

Figure 3-9. Schematic description of the experimental configuration used in adhesion force measurements to determine the effect of surface roughness.

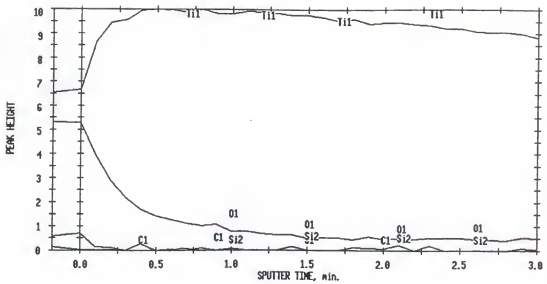

Figure 3-10. Auger Electron Spectroscopy of Si wafers.

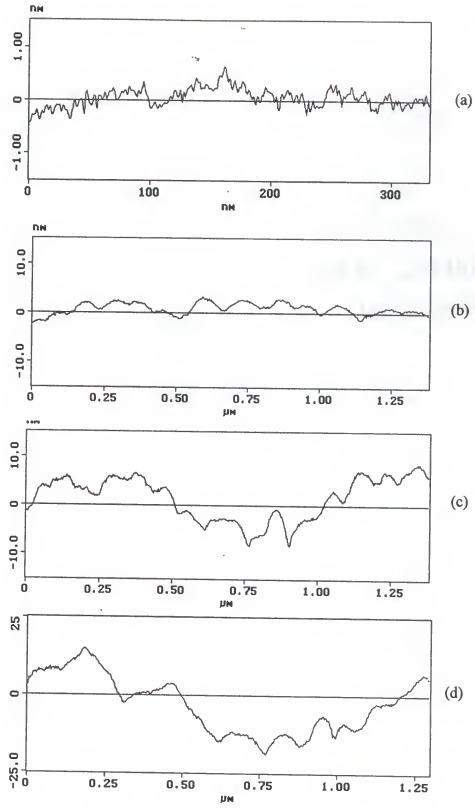

Figure 3-11. Surface roughness profiles of Ti-deposited Si wafers. a) Sample 1, b) Sample 2 c) Sample 3 and d) Sample 4.

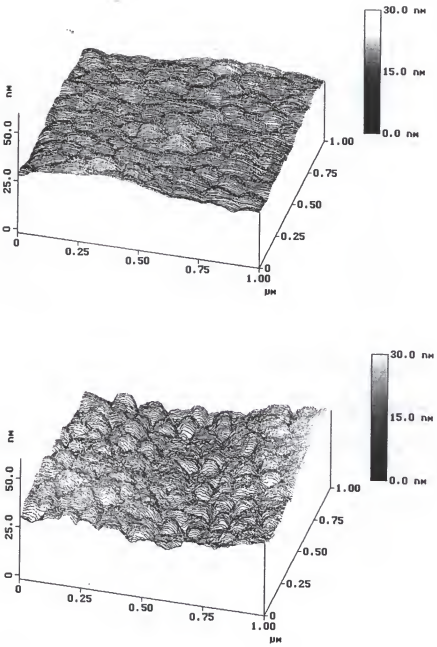

Figure 3-12. Surface topography of samples a)#2 and b)#4.

CHAPTER 4
RESULTS

Operating Parameters, Process Optimization

Processing Time

Overall, the MAIC process was observed to have short processing times, generally not exceeding 10 min. Since the frequency of collisions increases with time, processing time is a major variable controlling the coating process. The time effect was investigated by conducting 5 experiments for different times, 1, 3, 5, 7 and 10 minutes. PMMA and AKP 50-Al_2O_3 were used as primary particles and secondary particles, respectively. A graph of surface coverage (%) as a function of processing time is shown in figure 4-1. The surface coverage was determined by line analysis technique on the SEM pictures. 10 different lines of 8 cm was drawn on each SEM image. The length where line crosses the alumina particles were divided to the total length. The average of 10 lines gives the total surface coverage. A maximum surface coverage (70%) was observed for samples coated for 5 min. No remarkable improvement was observed in the surface coverage of

primary particles for longer processing times. The process reached a saturation limit after 5 min.

SEM images of the samples for 1 min, 3 min and 5 min treatment intervals are shown in figure 4-2. In the initial stages of the process, alumina secondaries are highly agglomerated and spread on the surface of PMMA primaries as can be seen in 1 min treated sample. The percentage of agglomerates reduces in size and in number as the process continues and eventually a homogeneously distributed surface, is obtained. A similar behavior was observed for nanosized silver particles (~50 nm) coated on Al_2O_3 (20 μm) primaries for 1, 3 and 5 min. Figure 4-3 shows silver particles stays as agglomerated at 1 min sample and then almost no agglomerates are seen on the SEM image of 5 min MAIC treatment.

Current and frequency

The effect of current on the coating efficiency was obtained by varying current passing through the electromagnets at a fixed frequency of 45 Hz. It was found that the surface coverage for PMMA/Alumina system mentioned above increased with increase in current as shown in figure 4-4. The maximum current applied was 5 amperes.

Using an optimum current of 5 amperes, the frequency of the system was varied from 45 Hz to 100 Hz and the surface coverage was monitored. An approximately sinusoidal type

periodic behavior was observed as shown in figure 4-5. Surface coverage first decreased from 45 to 70 Hz. At higher frequencies it increased and finally attained a saturated value at 90 Hz. Indication of another decrease cycle was observed after 100 Hz.

The amount of magnetic particles

Various magnet to powder (PMMA/AKP-50 system) ratios were used to determine the optimum mass of magnets to be used in the MAIC process. The magnet/powder mass ratios of differing proportions were used in the MAIC process and the results obtained are shown in figure 4-6. As the magnet to powder ratio was increased, the percentage coverage with secondary particles was increased too. There was not any remarkable increase for magnet/powder ratios greater than 2. Therefore, an optimum magnet/powder ratio was found as 2 and the rest of the experiments were conducted using this ratio.

The Effect of Particle Size

Figure 4-7 shows the surface coverage of AKP-50 Al_2O_3 secondary particles on PMMA and alumina primary particles as a function of secondary particle size. The figure shows a relatively higher degree of surface coverage when the size of secondary particles is below 0.4 μm. However, the surface

coverage on alumina core particles was quite low for all secondary particle sizes. The SEM pictures regarding the surface coverage for the secondary sizes of 0.2 μm and 1 μm are shown in figure 4-8.

Poor surface coverage was obtained when using very large primary particles such as greater than 1000 μm.

The adhesion forces as measured by AFM as a function of particle size are shown in figure 4-9. The forces measured for an AFM tip of nearly 0.1 μm in size were observed to be much higher than the ones observed for sphere interaction.

The Effect of Humidity

A uniform, non-agglomerated and high degree of surface coverage was obtained at low relative humidities such as 20% as shown in the SEM image of figure 4-10(a) for MAIC treated PMMA and AKP-50 alumina system. Increasing the humidity to higher levels i.e 80% resulted in poor surface coverage and more agglomeration at the surface of primary particles as shown in figure 4-10(b). The figure indicates a 80 % surface coverage for 20 % relative humidity and 20% surface coverage for 80% relative humidity.

In the second part of the humidity study, the change in

adhesion forces at different humidity levels was measured as a function of loading force. The results are shown in figure 4-11 for Al_2O_3 and in figure 4-12 for silver flat substrates. As was mentioned in the experimental part of chapter 3, a glass sphere of 10 μm radius having low roughness was attached to the AFM tip and brought into contact with alumina and silver substrates.

Figure 4-11 shows that the normalized force value on alumina flat surface rises from 300 mN/m levels to 550 mN/m around a critical humidity range of 40% RH indicating liquid bridge formations and as a result, strong capillary forces acting on the particle.

For the silver substrate, the critical humidity range, where adhesion forces abruptly increases, was observed around 60% as shown in figure 4-12. The adhesion force behavior as shown in this figure is different from alumina for the same range of applied force. The adhesion forces steadily increases up to a constant value then stays the same (plateau) at low loading forces (L/R<4 mN/m) at high humidity range 60-70% for silver substrates. However, the adhesion force is independent of loading force above L/R 1-2 N/m at all humidity levels for Al_2O_3 substrate.

In the literature there is a vast amount of information on the adhesion forces in humid environments without taking

roughness into consideration. The effect of humidity on the adhesion force for rough samples was investigated on the silicon wafer samples having controlled rough surfaces. Figure 4-13 suggests that there seems to be a difference between dry and humid adhesion forces within small deviations from smooth surface ideal value i.e., within 1 nm RMS range. Since the experiments were conducted on the same sample there is no standard deviation in the horizontal x-axis. An average of 10% standard deviation was observed in force values. The difference reduces at large roughness ranges.

The Effect of Loading Force

Systematic measurement on PMMA (H_v=20) and alumina (H_v=2100) substrates show that the adhesion force increases as the applied load increases for PMMA, whereas the adhesion force is independent of the applied load for alumina substrate. Figure 4-14 shows the adhesion force results for both substrates. Alumina and PMMA surfaces were chosen such that the mean roughness value of both are very close to each other so that, the elasticity or hardness is the major variable affecting the results.

Besides AFM experiments, the effect of using soft PMMA and hard alumina as primary particle surfaces was investigated using MAIC experiments. AKP-50 Al_2O_3 was used as secondary

particles for both primary particles. The samples were ultrasonicated before SEM pictures are taken. In the case where PMMA was used as primary particles, the alumina coated layer was remained without too many particles detached as shown in figure 4-15(a), whereas, the secondary particles were almost completely detached from the alumina primary surfaces as shown in figure 4-15(b). The results are complementary to the observed increased adhesion for PMMA surfaces upon the application of external loading.

Each collision leads to an impact or sudden external pressures on the primary surface in the MAIC experimental conditions. In that sense the static conditions of AFM experiments are alike with MAIC system experimental conditions.

The Effect of Surface Roughness

The change in adhesion forces upon very small, nano-scale deviations from ideal smooth surface topography were calculated for the tip and glass sphere experimental configurations, respectively. 3-D graphs need to be used because the abscissa has two values RMS_1 and RMS_2 which are more proper representation of surface roughness. A sharp drop in adhesion force was observed within 1-2 nm RMS roughness range on Ti-deposited Si wafer surfaces which were mentioned

in chapter 3. The force then stayed more or less constant upon further increase in roughness as shown in figure 4-16.

The experimental results obtained were compared to the existing adhesion force models for rough surfaces of equations (2.12) and (2.13). The most widely used model in the literature is the Rumpf [Rum75] approach considering roughness as a semi-sphere with radius r as shown in figure 4-17. It is difficult, however, to measure the value of r experimentally. Moreover, real roughness significantly deviates from the representation by radius of asperity peak. All the roughness data obtained through AFM measurements is expressed as RMS (root mean square) which is a statistical parameter. Therefore the equation in Rumpf's model as given in equation (2.12) was modified to be able to express roughness as RMS for comparison purposes.

From geometrical configuration and definition of RMS a relationship was developed between r and RMS as explained below:

Coordinates r_1 and y in figure 4-18 can be related to spherical coordinates r and α:

$r_1 = r \cos\alpha$

$y = r \sin\alpha$

According to the general definition,

$$RMS^2 = \int_0^{\lambda/4} \frac{y^2 r_1 dr_1}{\pi(\lambda / 4)^2} k_p$$

where $\lambda=4r$ is the wavelength of roughness and k_p, 0.907 is the surface packing density. Substituting r_1 and y in RMS; RMS=0.603r is obtained or r=1.485 RMS. Rumpf's equation as given in chapter 2 (eq. 2.12) was modified by inserting r and replacing it with RMS. As a result, the following equation is obtained:

$$F_{ad} = \frac{AR}{6Z_0^2}\left[\frac{1}{1 + R / (1.485RMS)} + \frac{1}{(1 + 1.485RMS / H_0)^2}\right] \quad (4.1)$$

Figure 4-16 shows a comparison between Rumpf's model and experimental data obtained from the interaction of a glass sphere with the Si wafer surfaces. In drawing the graph, a total value of RMS = $\sqrt{RMS_1^2 + RMS_2^2}$ was taken. A value of the Hamaker constant, A=1x10^{-19} J was used for calculations. As can be seen from figure 4-16, there is a significant difference in adhesion forces calculated from modified Rumpf's approach and the AFM experimental adhesion force measurements in this study. The major problem in quantification of the influence of surface roughness on adhesion is that surface roughness is difficult to describe which is the possible reason for the discrepancy in the measurements.

Alternative roughness models were developed to minimize

the difference between theoretical calculations and experimental results. The models use not only the radius of asperity peak but also the wavelength which provides more accurate information about roughness and will be discussed in chapter 5.

The Effect of Low Pressures

For the development of an advanced technology to manufacture composite particles with a uniformly thick coating layer, it is required to determine the mechanism and effect of vacuum on composite particle formation. Composite particles synthesized under low pressure conditions were observed to have uniform and almost agglomerate free surfaces. SEM images of samples processed at pressures of 100 mTorr and 700 mTorr are shown in figure 4-18(a) and 4-18(b) for PMMA/AKP-50 alumina system. The SEM image of the MAIC experiment run under normal atmospheric conditions is shown in figure 4-18(c). The surface coverage and uniformity of the low pressure coated surfaces were much higher than ambient atmosphere coated samples. Although a few agglomerates were observed at 700 mTorr, they were eliminated at 100 mTorr and a uniform which does not have any segregated or patched regions of alumina secondaries on PMMA was obtained.

The samples obtained after low pressure coating and

normal atmosphere conditions were put into ultrasonication bath to compare the strength of adhesion. There was not any significant reduction in surface coverage of low pressure coated samples after ultrasonication.

The Role of Velocity

Fluidization of particles in the MAIC system is provided by haphazard motion of magnetic particles. Therefore, the velocity of magnetic particles was studied with a high speed camera. It was found that the magnetic particles have high rotational speeds, 70-100 rev/sec, in addition to their translational velocities 30-60 cm/sec. Rotational and translational velocities were measured as a function of frequency of the current.

The influence of magnetic particle translational and rotational speeds on the surface coverage was analyzed. Figure 4-19 shows that the rotational motion of magnetic particles increases the surface coverage whereas increasing translational velocity does not seem to have any significant effect on the surface coverage. There is no indication of any trend or slope was seen on the translational velocity versus surface coverage plot.

Collision frequency

MAIC processing chamber includes nearly 10^{11} secondary, 10^7 primary and 10^2-10^4 magnetic particles. Although the number of magnetic particles are less than the number of other particles, they are the main fluidizing agent of the MAIC process. Therefore, their collision frequency is determining factor in the overall efficiency of the process. Equation 3-1 was used in the calculations. The frequency was varied by varying the number of magnetic particles and keeping the amount constant. Since the frequency of the magnetic field or current in the electromagnets was not changed, the velocity is also kept constant at around 40-50 cm/sec. The results are shown in figure 4-20 for alumina core particles coated with AKP-50 secondaries. Increasing the frequency of magnetic particles resulted in a significant improvement in the surface coverage of primary particles. The SEM pictures corresponding to a low ($4x10^6$) and high collision frequency ($1.2x10^{10}$) experiments are shown in figure 4-21. Although coating alumina on alumina is a difficult task due to non-deformable nature of the surface, high collision frequency yielded a satisfactory coating.

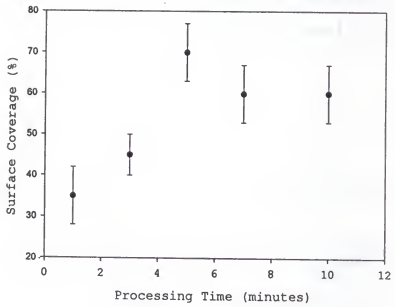

Figure 4-1. Surface coverage vs processing time for PMMA/Alumina primary-secondary particle combination.

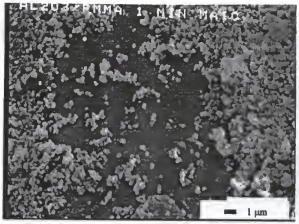

(a)

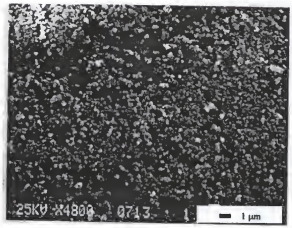

(b)

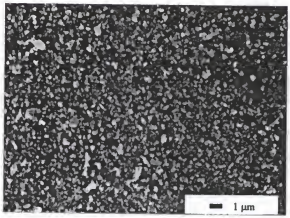

(c)

Figure 4-2. SEM pictures of Alumina coated PMMA particles: (a) for 1 min; (b) for 3 min and (c) for 5 min.

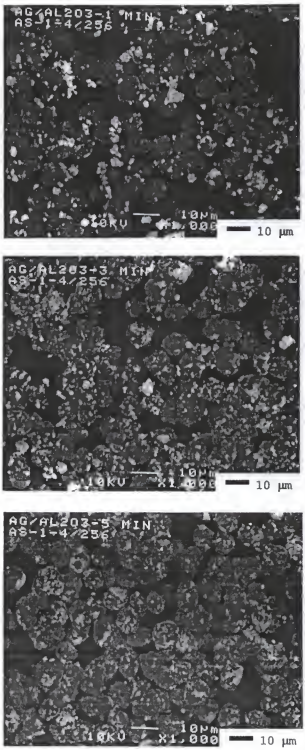

Figure 4-3. SEM pictures of Ag coated Al_2O_3 particles: (a) for 1 min; (b) for 3 min and (c) for 5 min.

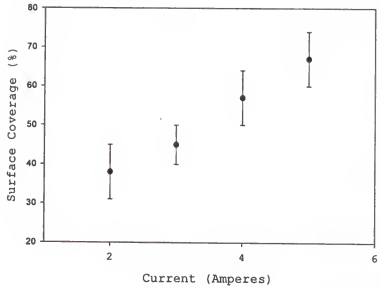

Figure 4-4. Surface coverage as a function of current for 5 min MAIC treated PMMA/Alumina sample.

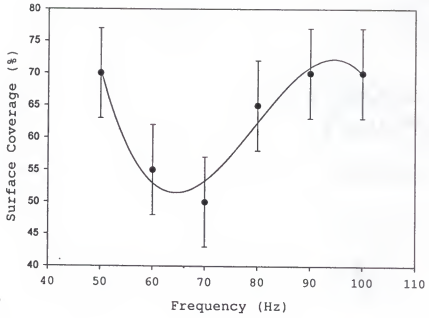

Figure 4-5. Surface coverage as a function of frequency for 5 min MAIC treated PMMA/Alumina sample.

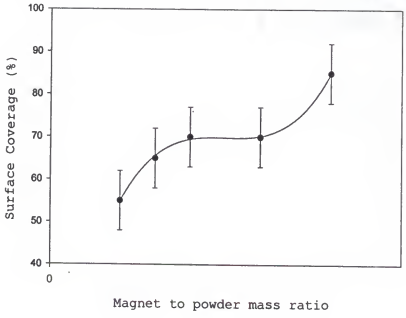

Figure 4-6. Surface coverage as a function of magnet/powder ratio for 5 min MAIC treated PMMA/Alumina sample.

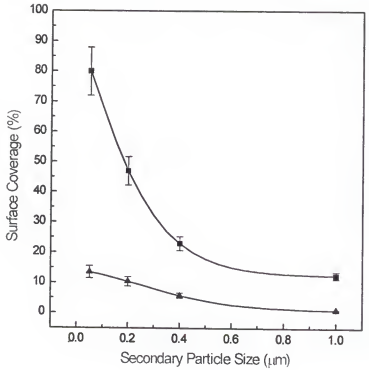

Figure 4-7. The effect of size of secondary particles on surface coverage for 5 min processing time, magnet/powder ratio 2.

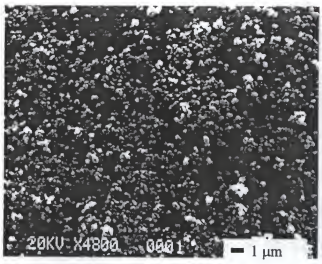

(a)

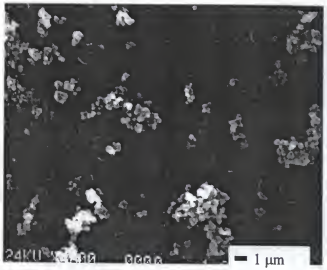

(b)

Figure 4-8. Surface coverage of PMMA as a function of alumina at different sizes a) 0.2 µm b) 1 µm for 5 min MAIC treated samples.

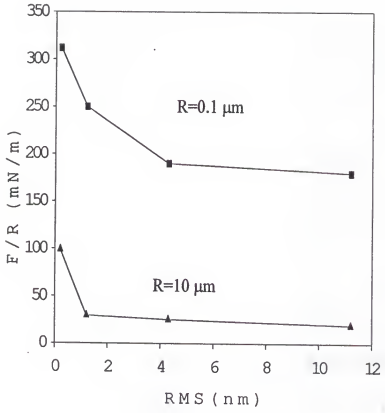

Figure 4-9. AFM force measurement on a silicon substrate having various roughness values for two different particle radii.

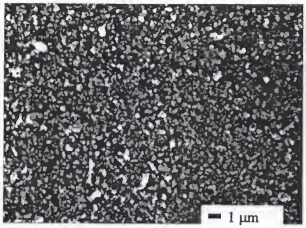

(a)

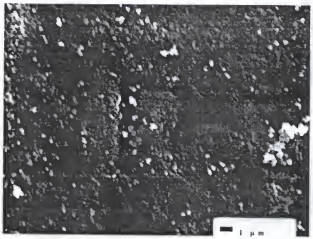

(b)

Figure 4-10. Surface coverage on MAIC treated PMMA/Alumina system at a)20% b)80% relative humidity.

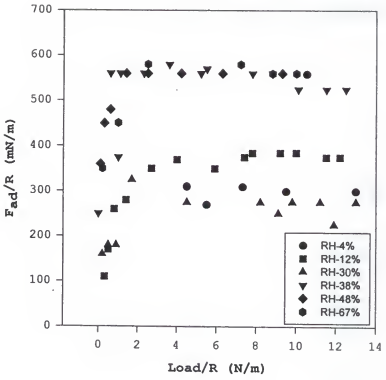

Figure 4-11. Adhesion force measurements on alumina substrate surface at various humidity levels.

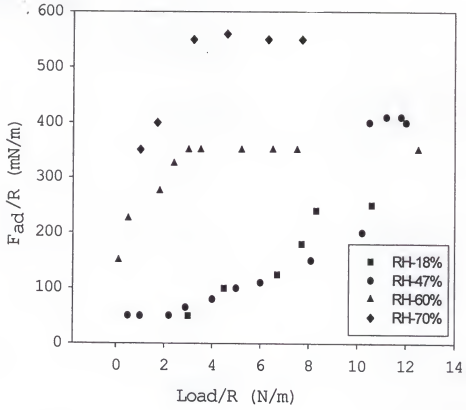

Figure 4-12. Adhesion force measurement on silver substrate surface at various humidity levels.

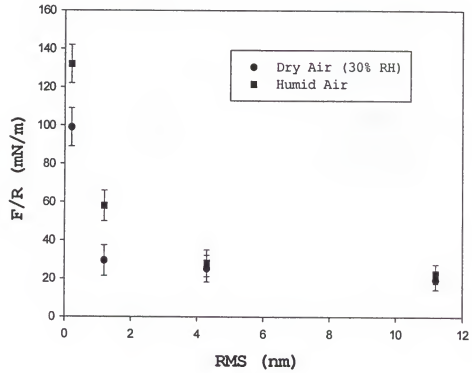

Figure 4-13. Adhesion forces measured in dry and humid environments as a function of roughness.

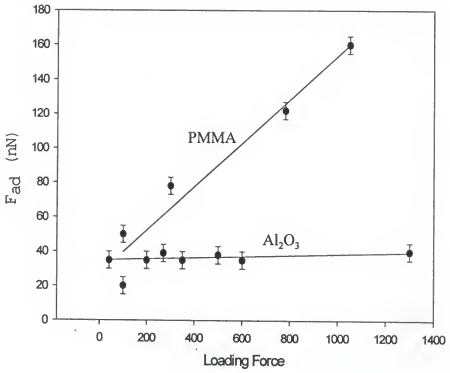

Figure 4-14. The adhesion force between AFM tip and PMMA and alumina substrates.

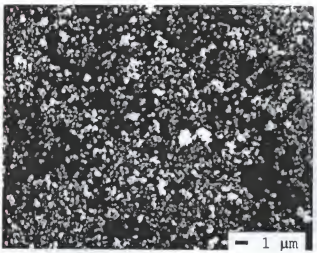

(a)

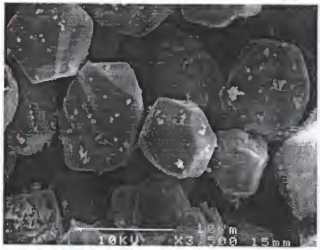

(b)

Figure 4-15. SEM pictures of alumina coated a) PMMA b) Alumina primary particles following an ultrasonication treatment for 20 sec after 5 min MAIC processing.

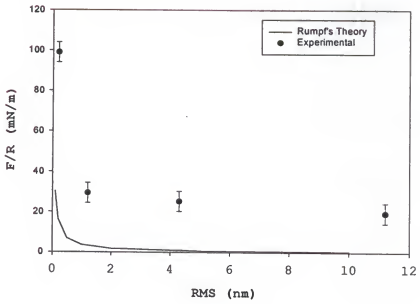

Figure 4-16. Comparison of experimental data with the Rumpf's model.

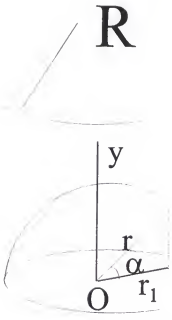

Figure 4-17. Roughness profile suggested by Rumpf.

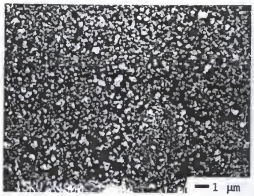

(a)

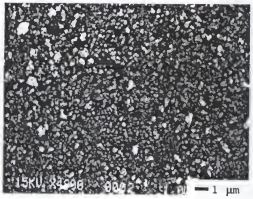

(b)

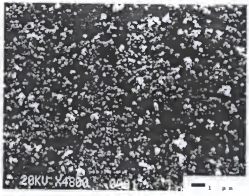

(c)

Figure 4-18. SEM pictures of PMMA/Alumina samples treated at different pressures;
a)100 mTorr b)700 mTorr c)Ambient atmosphere

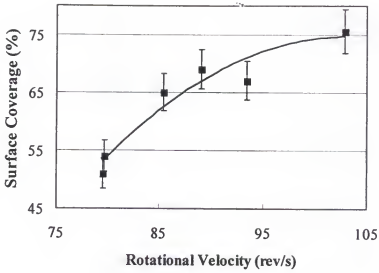

(a)

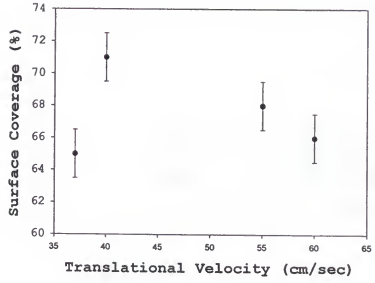

(b)

Figure 4-19. Surface coverage change in PMMA/Alumina system as a function of a)rotational b)translational velocity changes.

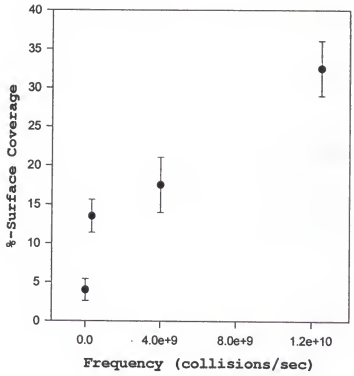

Figure 4-20. The effect of collision frequency of magnetic particles on the surface coverage for alumina secondary particles coated on alumina primaries.

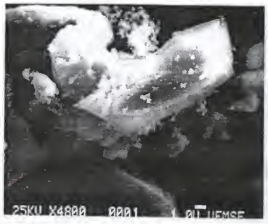

(a)

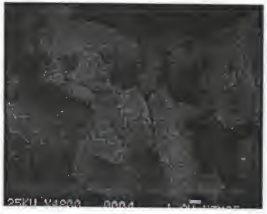

(b)

Figure 4-21. SEM pictures of alumina coated alumina primary particles a) low frequency ($4x10^6$) b) high frequency ($1.2x10^{10}$) collision regimes.

CHAPTER 5
DISCUSSION

Composite Formation and Mechanism of the Process

As received secondary particles are in agglomerated form due to their small sizes. Typical agglomerate size varies from 10-20 μm as shown in figure 5-1. Although being practical, dry coating techniques remains challenging because of difficulty in dispersing agglomerates.

In MAIC processing, agglomerates form an ordered mixture around primaries in the initial stages of the process as can be seen in 1 minute treated samples in figure 4-2. As mentioned earlier, large differences in the particle sizes and adhesion among the particles cause an ordered arrangement of particles [Her75]. The agglomerate size reduces constantly because of the collision process taking place. The comparison of SEM images for 1, 3 and 5 min samples of figure 4-2 shows a significant reduction in the size of agglomerates. Ordered mixtures generally forms in two distinct stages [Ste80]. In the first stage, a single secondary particle forms from

agglomerate. The rate at which this occurs depends on the rate of energy input arising from collisions causing the momentum changes in the primary particles. In the second stage, the single secondary particle adheres on the primary surface. Secondary particles separated from their agglomerates have clean, uncontaminated and therefore, highly energetic surfaces. As a result, they strongly adhere to primary surfaces.

Sometimes embedding was observed due to external forces generating micro-fragments of particles during impaction. A much higher degree of embedding was observed for 50 nm Al_2O_3 secondaries due to their small size.

Since the MAIC process is a collision process, both attachment and detachment is possible. Once the primary surface has been covered to a large degree, the probability of detachment increases compared to attachment. Incoming secondary particles will less likely to find a fresh surface to adhere. Therefore a small drop in surface coverage in longer processing times samples can sometimes take place.

A simple model explaining the mechanism of the MAIC process is shown in figure 5-2. There are three stages during processing. In stage I, an ordered mixture forms. In stage II, agglomerates around the primary surface were broken by the colliding magnetic and primary particles. In stage III,

secondary particles which are separated from their agglomerates adhere to the surface. Eventually, uniform homogeneous composite particles are obtained. Further treatment causes the process to enter into a detachment dominated regime.

During the process, magnetic particles are also coated which is not a serious problem because it does not create any contamination as long as the same kind of magnets are used for each application.

Particle Size Effect

MAIC experiments have shown that changing the size of secondaries has much greater impact on the composite formation than changing the size of primaries. Figure 5-3 explains how the adhesion force changes by changing the size of secondary particles [Kap98]. Primary particles on the other hand, have a retarding effect on the fluidization in the chamber when they exceed a size range causing very poor surface coverage. A more stronger magnetic field is needed for fluidization in that case. Figure 4-7 shows the effect of changing the size of secondary particles on the coating efficiency. The data in figure 4-7 look like, they contradict the adhesion theory which predicts higher adhesion forces for larger particle sizes. Adhesion forces according to two fundamental adhesion

theories, JKR (Johnson-Kendal-Roberts) and van der Waals are linearly dependent on particle size as shown in the equations below.

$$F_{vdw} = \frac{AR}{6Z_0^2} \quad \text{(VdW)} \qquad F_{JKR} = \frac{3}{2}\pi\Delta\gamma R \quad \text{(JKR)}$$

where A is Hamaker constant, Z_0 is the intermolecular distance separating interacting solids and γ is the surface energy term. There are a couple of explanations to attribute for such an observation. The first one is that the tangential removal forces have particle size dependency to the third power that is, $F=(4/3)\pi aR^3$ where *a* is the acceleration. Therefore as the size increases, the removal force acting on the particle increases more than the adhesion force. Secondly, the volume of secondary particles exposed to collisions gets larger and causes a higher probability for removal. The third reason might be the small particle sizes are less likely to be touched and removed either due to hydrated layer around the primary particle or surface undulations.

In the MAIC process particles below 0.4 μm was observed to be more protected against mechanical removal forces resulting from impaction.

The Effect of Humidity

At low relative humidities, the moisture associated with the particles is adsorbed water vapor of having a thickness ≈0.3 nm [Got95]. The thickness of the layer increases as the humidity increases. Eventually, liquid bridges form at points of contact with other particles at a critical humidity. Capillary forces start acting between particles due to liquid bridges. In this section, the interparticle forces due to liquid bridges and their effect on the MAIC process are investigated. Some consideration is given to how these forces depend on the contact geometry.

MAIC experiments using PMMA primary particles and AKP-50 alumina secondaries was conducted at varying humidities to observe the evolution of coating on PMMA. Poor surface coverage was observed at high humidity ranges 70 and 80% RH as shown in figure 4-10. The result can be attributed to increasing size of secondary particles as the relative humidity increases.

The existence of capillary forces that are four times larger than van der Waals forces promotes an agglomeration process rather than adhesion among the secondary particles. Thus, secondary particles form stronger agglomerates and

increase in size. The relative size of secondary particles eventually reaches to a critical size that can possibly be removed by mechanical forces. In addition, the increased thickness of the adsorbed water layer on the primary particles at high humidities acts like a lubricant and results in secondary particles experiencing more difficulty in penetrating and reaching the primary particle surface. It prevents particles to form a dry contact or mechanically interlock to the surface.

Flow and mixing behavior of powders (salicylic acid of 3.5 μm and sucrose crystals of 400 μm) under different humidity conditions was studied by Stephenson et al. [Ste80]. The result for 84% relative humidity indicated considerable moisture bonding and sticky flow supporting the poor surface coverage obtained in the MAIC process above 70-80% relative humidity. Turner and Balasubramanian reported 65% RH as the lower limit for capillary forces playing part in particle adhesion [Tur74]. Harnby et al. reported a critical relative humidity of 60-70% for glass particles. The values reported in the literature mainly comes from tensile test measurements, centrifuge or optical observations.

Direct adhesion force measurements were performed in this research to determine the critical humidity range more accurately and to quantify the forces associated with humidity

changes by using the AFM.

The results from contacting a 10μm glass sphere with PMMA and silver substrates are shown in figures 4-11 and 4-12, respectively. The adhesion force change at different humidities was drawn as a function of loading or applied pressure. The adhesion and loading forces are normalized with radius to eliminate the effect of radius of sphere on the results. Therefore, load/radius (L/R) and adhesion force/radius (F_{ad}/r) were used in the graphs.

In figure 4-11, the adhesion force is practically independent of loading force (L/R) at every humidity level when L/R>1-2 N/m. The independence can be explained by the non-deformable nature of both glass and alumina surfaces in the applied range of L/R<12 N/m or L<10^{-4} N. On the other hand the result indicates a weak dependency of adhesion force to elastic deformation of samples.

It appears from figure 4-11 that there are two ranges of humidity: one is below 30% RH range, the other is above 48% RH range. Notice that, there is a difference between critical humidity ranges observed in the MAIC experimental conditions and AFM force measurements. The MAIC range corresponds to near 70% RH which is consistent with the values observed in the literature such as reported by Harnby et al. as shown in figure 5-4. On the other hand force measurements with AFM

gave a critical range around 40% RH. The difference might be attributed to the dynamic and static conditions of MAIC and AFM, respectively. Dynamic conditions might involve viscosity effects in the bulk of meniscus. In addition, the AFM is a single particle measurement while, many particles are involved in case of the MAIC processing.

In the low humidity range below 30% RH of figure 4-9, the adhesion force is relatively weak, F/R=300 mN/m, which can be related to dry contact van der Waals forces with Hamaker constant near $A=1.6\times10^{-19}$. The theoretical value of F_{ad}/R for van der Waals force is 200 mN/m. The overestimated force found in the experimental data indicates the action of an additional force besides dispersion forces. It might be as a result of formation of acid/base interactions. Even at very low humidity levels, a mono or double layer of water molecules are adsorbed which is different than the bulk water. The layer is not condensed enough to form bridging at that stage [Got95]. This short range polar forces can be one of the strong reasons for the total adhesion force to be larger than the theoretical van der Waals value. Similarly, Chikazawa et al. detected the same type of behavior at humidities as low as 20% RH by studying porous glass particles. It was presumed that this was due to the formation of hydrogen bonds [Chi84]. They also observed a marked increase in adhesion force in the

region 60-80% RH. The increase was explained in terms of the change in the adhesion mechanism from hydrogen bonding to liquid bridge formation.

In the higher humidity above 48% RH range, a sudden increase in adhesion forces from 300 to 550 mN/m was observed as shown in figure 4-9. 500mN/m value is close enough to the theoretical capillary force value of 810 mN/m. One can assume confidently that the main contribution to adhesion force at higher humidities above L/R>2 N/m is a result of capillary forces. The difference between the theoretical value and the experimental can be explained quantitatively by the role of roughness.

There are very few studies regarding the role of surface roughness on the forces of adhesion in humid environments. Harnby et al. reported that surface roughness has a much greater significance on the adhesion at relative humidity values less than the critical humidity range using rough stainless steel surfaces and glass particles as shown in figure 5-5.

An in-depth investigation of the effect of roughness on the capillary force was performed in this research considering the geometry of the contact area. The interaction of a smooth sphere (roughness<1 nm) with a rough flat surface in the presence of humidity was analyzed.

There are two possible geometrical configurations for the meniscus existing between a rough flat surface and a smooth sphere. Figure 5-6(a) shows the first case where $2r>y_{max}$ where r is the radius of meniscus and y_{max} is the height of roughness peak. In the second case in figure 5-6(b) the meniscus forms between the roughness peak and sphere rather than between sphere and flat surface.

In the first case where $2r>y_{max}$, one may think the same force acts as in smooth solids. However, the distance between the smooth sphere and flat surface increases because of the existence of the asperity peak touching the sphere. This changes the area of the liquid bridge. Thus, the adhesion force according to equation 2.11 ($F_{ad}=\Delta P x Area$) also changes. The Laplace pressure term ΔP in the equation does not change because, according to Young-Laplace equation (2.10) ΔP depends on the radius of the meniscus where the radius of the meniscus only depends on the relative humidity and surface energy of interacting bodies. The Kelvin equation as shown below in equation 5-1 states that the radius of meniscus, r is independent of the distance between the sphere and flat surface.

$$r = \frac{-V_{mol}\gamma}{RT\ln\psi} \qquad (5.1)$$

where V_{mol} is the molar volume of water and ψ is the relative humidity.

Therefore in order to calculate the adhesion force for this configuration the area of bridge under the smooth sphere must be calculated. For simplicity, the thickness of adsorbed layer is neglected.

From figure 5-6(a), [OC]=R+D(height of asperity)

$$[OC]=(R+r)\cos\varphi+r \tag{5.2}$$

Where φ is the angle embracing the meniscus. Assuming R>>r and φ<<1, the following expression is obtained;

$$\varphi=\sqrt{\frac{2(2r-D)}{R}}. \tag{5.3}$$

The area of bridge or meniscus is equal to

$$S=\pi[BA]^2. \tag{5.4}$$

$$[BA]=R\ (\sin\varphi)=R\ \varphi \tag{5.5}$$

Substituting equations 5.3 and 5.5 in 5.4 we obtain;

$$S=2\pi R(2r-D). \tag{5.6}$$

Thus, using equation 2.11 where $F_{ad}=\Delta P x S$, we obtain the adhesion force for humid environments in the presence of surface asperity as;

$$F_{ad}=4\pi\gamma R(1-D/2r) \tag{5.7}$$

The discrepancy between observed (550 mN/m) and theoretical (790 mN/m) values of adhesion forces in the case

of the alumina flat substrate and the glass sphere interaction can be explained with the above equation (5.7). The surface roughness of alumina measured with the AFM and found to be as RMS=0.4 nm (can be called a smooth surface). The radius of meniscus calculated from the Kelvin equation is 0.78 nm for 48% RH. Substituting the data in equation 5.7 a value of adhesion force 587 mN/m is obtained which is very close to the experimentally observed value 550 mN/m.

In case where $r<y_{max}$, equation 2-13, $F_{ad}=2\pi\gamma R(\cos\theta_1+\cos\theta_2)$, is valid but the radius of asperity peak (r_p) should be used rather than the radius of interacting sphere, *R*.

AFM force measurements were conducted on soft silver flat surfaces, under the same conditions as mentioned above for the alumina flat surfaces in order to observe the contribution of substrate properties on the results. A spherical glass sphere was contacted to a silver flat surface at different loads and humidities. The results, as shown in figure 4-12, suggest that at low loading forces, L/R<4 mN/m, and in the high humidity range of 60-70%RH, the adhesion force steadily increases and reaches a plateau value. The rise for the silver substrate is in a more gradual manner than for the alumina substrate. This type of increase can be explained by the plasticity of silver.

At low humidity levels, roughness prevents the formation

of a water meniscus. Increasing the loading force suppresses the asperity peaks and capillary forces become active again. The adhesion values increase to 350-550 mN/m and come close to experimental values observed for the alumina substrate.

At high humidity ranges 60-70% RH, the radius of meniscus as measured by the Kelvin equation (V_{mol} and γ of water is known and ψ is relative humidity term that is 0.6 and 0.7 for this case) is 1.04-1.4 nm. The roughness of the silver substrate is measured to be 3 nm (RMS). As explained above when the radius of meniscus is smaller than the roughness or the height of the asperity peak, water bridges cannot form between sphere and the substrate, instead, they form between asperity peak and substrate as shown in figure 5-6(b). The adhesion force in this case can be calculated according to equation $F_{ad}=2\pi\gamma r_p(\cos\theta_1+\cos\theta_2)$.

The Effect of Loading Force

The adhesion force between a particle and a substrate for elastic and inelastic contacts is schematically drawn in figure 5-7. Plastic or viscoelastic deformation causes the formation of a surface between two interacting bodies as shown in figure 5-7(b). Elastic deformation on the other hand, produces a point contact as shown in figure 5-7(a). The van

der Waals adhesion force equations are expressed as

$F_{ad} = \frac{AR}{6Z_0^2}$ and $F_{ad} = \frac{AS}{6\pi Z_0^3}$ for point contact and for surface

contact; resembling elastic and inelastic deformations respectively. Comparing both equations, the adhesion force due to inelastic deformation increases by a factor of $S/(\pi Z_0 R)$. The same result also was found by Xie [Xie97] calculating the total attractive energy using the van der Waals equation. A three orders of magnitude higher adhesion force is calculated in case of inelastic deformation considering a typical value of the Hamaker constant as $A=10^{-19}$ J and $Z_0=0.3$ nm for a particle embedded to a full radius.

Primary particles like glass beads, Al_2O_3 have hard surfaces and therefore make it difficult to produce inelastic deformations. The area of contact in such cases is small. On the other hand, soft, low yield point particles like PMMA ($H_v=20$) are easier to produce inelastic deformations. The area of contact is larger in this case and hence the adhesion forces are larger.

The effect of deformation is explained in the theory of Maugis and Pollock named the MP theory [Mau84] as was mentioned in chapter 2. The stresses generated become sufficiently large to exceed the yield strength of one of the

contacting materials. In that instance a totally or partially plastic deformation will occur. MP theory relates the external pressure to the yield strength as given in equation (2-18);

$$P+2\pi w_a R=3\pi a^2 Y$$

where Y is the yield strength of the yielding material, P is the external loading and w_a is the work of adhesion. The equation states that the area of contact increases as the yield stress decreases and can be used to predict the area of contact beyond that due to surface forces.

It is demonstrated in the previous chapters that by attaching a particle to AFM cantilever or using the tip, new information and insight into the particle-substrate interaction can be obtained. Figure 4-14 shows that the adhesion force increases as the external loading on the particle increases while the adhesion force on alumina stays unchanged. The results support the MP theory and give a large numerical discrepancy between materials of different yield strength. A similar study was performed by Schaefer et al.[Sch94] on the effect of loading force by interacting 5 μm polystyrene spheres with a p-type silicon flat substrate. Figure 5-8 shows that the adhesion force increases slightly with the loading force. Each data point represented an average of three independent measurements. The increase is

beyond the uncertainties of the measurement and is thought to reflect an increase of adhesion due to the applied external load. If the system is governed by elastic behavior, the force of adhesion should be independent of loading due to elastic rebound of the materials. It was concluded that the observed non-linearity is due to either a viscoelastic or an inelastic response of the particles to external loading.

The magnitude of adhesion forces are close to each other between this research and Schaefer's work. However, the increase in adhesion due to deformation is much more pronounced in the experimental results of this study due to larger loading forces used in the range 100-1000 nN compared to 50-400 nN. Besides low loading forces, elastic flattening also might contribute rather than plastic deformation. Elastic flattening especially in polymers is a considerable factor as reported by Tsai et al. [Tsa91].

The pressure range applied in this research, 100-1000 nN creates a plastically deformed area of $500\text{-}5000 \times 10^{-18}$. An adhesion force in the range 30-300 nN is required to create such an area of deformation. The resultant range (30-300 nN) is within the range experimentally obtained on PMMA substrates (20-160 nN) as shown in figure 4-14. The theoretical calculation was done according to the equation, $F_{ad} = \frac{AS}{6\pi Z_0^3}$.

Therefore, the experimental range is enough to create plastic deformation and the higher adhesion force is from the contribution of plastic deformation.

In the MAIC experiments conducted using PMMA, glass and alumina as primary particles, the PMMA surface coverage was seen to be much higher than alumina or glass surface coverage. Surface coverage on PMMA partly remained even after ultrasonication indicating the strength of coating and plastic deformation. In the case of glass and alumina particles surface coverage was almost totally removed after ultrasonication due to the elastic nature of adhesive bond.

Surface Roughness Effect

A significant difference in the adhesion force was observed between the experimental results on the controlled rough samples mentioned in chapter 3 and the Rumpf's theory which is widely used in the literature. The reason can be attributed to the under-estimated radii of peaks in Rumpf's model, which does not take the wave length of the asperity into account and depends only on one profile parameter, namely, the radius of the peak as shown in figure 4-17. In general, at the very least, two parameters and their associated numerical values are necessary to properly define

roughness [Bri94].

In that regard, a roughness model was suggested considering roughness as a wave with an amplitude y_{max} and wavelength λ as shown in figure 5-10. Here r is the radius of peak, R is radius of sphere, α_0 is half an angle embracing peak.

Adhesion force, F_{ad}, can be calculated with the following equation by considering the contact and non-contact van der Waals forces as in the Rumpf's study [Rum75]:

$$F_{ad} = \frac{AR}{6H_0^2}\left[\frac{r}{r+R} + \frac{1}{(1 + y_{max} / H_0)^2}\right] \tag{5.8}$$

The value of y_{max} is not an experimentally measurable parameter. However, it can be expressed in terms of another experimentally measurable parameter RMS from the geometry of the model in figure 5-10. The conversion is found as y_{max}= 1.817 RMS. The radius of peak is expressed in terms of λ and RMS as:

$$r=\lambda^2/(32k_1RMS) \tag{5.9}$$

The detailed calculation is given in appendix 5-1.

Substituting equation (5.9) and y_{max} the following equation is obtained:

$$F_{ad} = \frac{AR}{6H_0^2}\left[\frac{1}{1 + 32Rk_1RMS / \lambda^2} + \frac{1}{(1 + k_1RMS / H_0)^2}\right] \tag{5.10}$$

The first terms in brackets of equations (5.8) and (5.10) are related to contact interaction of the sphere with the peak, while the second terms are related to the non-contact interaction of the sphere with a flat surface.

Dependencies of total adhesion force and it's contact and non- contact components vs. RMS, calculated with equation (5.10), are presented in figure 5-11. It appears that contact interaction makes the main contribution in the range of large RMS, while at small RMS<1 nm the non-contact force is comparable or larger than the contact one. Thus, equation (5.10) predicts a sharp decrease of the adhesion force with increasing RMS in the low RMS range of a couple of nanometers, while at larger RMS the adhesion force decreases slowly.

Another way of considering roughness is shown in figure 5-12 in which Δ is the distance between the top of the peak and the "ideal boundary" (IB) of the surface which is the average distance from the substrate to the asperities. In the first approach the ideal boundary was coinciding with the real surface but in this approach it is not.

Assuming $\Delta = y_{max}/2 = (k_1 RMS)/2$ (5.11)

y_{max} was given as $y_{max} = 1.817$ RMS

For this model, F_{ad} is calculated with formula

$$F_{ad} = \frac{AR}{6H_0^2}\left[\frac{r}{r+R} + \frac{1}{(1+\Delta / H_0)^2}\right] \tag{5.12}$$

where, in agreement with equation (5.9),

$$r = \frac{\lambda^2}{(32k_1 RMS)}.$$

Substituting r and Δ in equation (5.12), an expression for the adhesion force is obtained:

$$F_{ad} = \frac{AR}{6H_0^2}\left[\frac{1}{1+32Rk_1 RMS / \lambda^2} + \frac{1}{(1+0.91RMS / H_0)^2}\right] \tag{5.13}$$

In figure 5-13 theoretical dependencies of adhesion force vs. RMS obtained from equation (5.10), equation (5.13) and Rumpf's model (equation 4-1) are shown. Note, that the wavelength λ is different for models in figures 5-10 and 5-12, namely, it is the distance between two neighboring peaks for the model in figure 5-10 and between each second peak for the model in figure 5-12. Figure 5-13 demonstrates that equations (5.10) and (5.13), suggested in this research, predict higher adhesion forces than modified Rumpf's equation as given in chapter 4, equation (4-1). It should be related to larger radius of the peak, calculated for equations (5.10) and (5.13), as compared with value of r calculated for corrected Rumpf's model for the same RMS. As can be seen from AFM

images of the wafer surfaces in figures 3-11 and 12, the surface roughness profiles can not be fit by any of the two models suggested above. Therefore, a double-wave profile, which is, closest to reality, as shown in figure 5-14, was suggested that represents mixture of the two approach suggested above. Equations regarding y_{max} for both models are still valid for each corresponding wave. However, in the framework of the model in figure 5-14, equation (5.10) and (5.13) are not valid anymore for but the following formula should be used instead;

$$F_{ad} = \frac{AR}{6H_0^2}\left[\frac{r_2}{R + r_2} + \frac{r_1}{(r_1 + R)(1 + \Delta / H_0)^2} + \frac{1}{(1 + (y_{1,max} + y_{2,max}) / H_0)^2}\right]$$

(5.14) or,

$$F_{ad} = \frac{AR}{6H_0^2}\left[\frac{1}{1 + 58R\ RMS_2 / \lambda_2^2} + \frac{1}{(1 + 58R\ RMS_1 / \lambda_1^2)(1 + 0.91RMS_2 / H_0)^2} + \frac{H_0^2}{(H_0 + 1.82RMS_1 + 1.82RMS_2)^2}\right]$$

(5.15)

In equations (5-14) and (5.15), the first, second and third terms in brackets correspond to the interaction of the sphere with the second roughness, first roughness and flat surface, respectively. These equations are valid if $r_{1,2} << R$. If $r_2 << R$, but $r_1 \not< R$; the interaction of sphere with flat

surface should be dropped, that is,

$$F_{ad} = \frac{AR}{6H_0^2}\left[\frac{1}{1 + 58R\ \ RMS_2 / \lambda_2^2} + \frac{1}{(1 + 58R\ \ RMS_1 / \lambda_1^2)(1 + 0.91RMS_2 / H_0)^2}\right]$$

(5.16)

The plastic deformation effect was ignored in the equations developed in the present study. A semi-quantitative evaluation was done for the contribution of the plastic deformation on adhesion force. This evaluation confirmed the relatively small role of plastic deformations for the hard materials used in this study.

Figure 5-15 shows a comparison between experimental data for adhesion forces measured by attaching a glass sphere on a cantilever beam and the theoretical surface drawn according to the double wave model proposed in this study. Experimental data supports the features predicted by present theory, that is, the sharp decrease in the adhesion force nearly by a factor of 5 within the first 1-2 nm increase in RMS, and the slow decrease of adhesion force for larger RMS. Quantitative agreement between theory and experimental data proves also that the adhesion force is related mainly to van der Waals forces for rough surfaces in dry air. Some experimental data points differ by almost twice that of the corresponding data on the theoretical surface F vs RMS_1 and RMS_2 in figure 5-15.

Besides the scattering of experimental data, the difference can be explained due to polar interactions which are not included in equation (5.16). The polar forces participate only in contact interaction and is significant at low RMS values. Another reason for the difference is the plastic deformation effect which is also not included in the equations. The total adhesion force includes both interactions. In addition, the adhesion force from equation (5.16) depends on the interaction of one peak with smooth sphere, while in reality several peaks can simultaneously contribute to adhesion force. Particularly, adhesion of particles in powder can include at least interaction of three peaks, which is minimum number of contacts for equilibrium.

Schaefer et al. [Sch95] obtained experimental values of an adhesion force much lower than theoretically calculated for smooth particles. Experimental values were found to be 50 times less than the theoretical values for smooth glass particles of 8 mm size. The theoretical calculation was based on the JKR model using the work of adhesion value from the literature. When the radius of asperity peak values were used for calculation rather than the radius of spheres, the discrepancy drops to 3 times. Actually, this last difference can be explained if it is considered that only van der Waals (dispersion) forces rather than polar forces contribute to the adhesion force at low loading levels. Note, that the asperity

heights in Schaefer's study are relatively high (10-20 nm) while in the present research they are 0.2-10 nm.

Besides the measurement of adhesion between wafer and glass sphere, the adhesion was also investigated between wafer and cantilever tip. In figure 5-16, the experimental results obtained are shown together with the theoretical surface calculated with equation (5.16). The radius of tip (R_{tip}) was taken as 100 nm in theoretical calculations. A qualitative agreement of experiments with theory was observed; for example, both theory and experiments for R= 100 nm give relatively high value of F_{ad} /R at large RMS as compared with adhesion force for R= 10 μm. The drop of experimental adhesion force when RMS increase from RMS 0.2 to 1-10 nm is not as high for tip (R= 100 nm) as the drop for the case of sphere with R=10 μm as can be seen by comparing figures 5-15 and 5-16.

The reason for the discrepancy between experimental and theoretical results in whole range of RMS for tip substrate interaction might be attributed to the small size of the tip which enables it to penetrate in between asperities and as a result tip interacts with several asperities rather than a single asperity.

The influence of roughness on non-contact long range van der Waals forces was studied theoretically by van Bree et al.

[Van74]. They reported a 25 % decrease of force for plane-sphere configuration for surface irregularities as small as 2 nm. This decrease in force is much lower than found experimentally in the present study. The reason of discrepancy between the present results and results of [Van74] is that all formulae in [Van74] were developed only for distances much larger than roughness and invalid for adhesion force, that is, for distances of order 0.3 nm. In the present work, the effect of roughness on non-contact forces was neglected suggesting that non-contact forces for large distances is much less than contact forces and the main contribution to adhesion for large distances comes from the contact forces.

Iida et al. [Iid93] have measured adhesion force for comparatively small roughness values but did not consider the non-contact adhesion term in their theoretical calculations. However, they have observed a similar type adhesion drop as a function of roughness that is, a sharp decrease within nano-meter range and a steady and gradual decrease afterwards which was also seen in the present work. Similar to Fuller and Tabor [Ful75], roughness was characterized by the STM using center line average values and the force of adhesion was measured by the impact separation method. The method measures average adhesive forces for 50% of the particles remaining on the substrate after separation.

Recently, Xie [Xie97] also carried out a theoretical study for the effect of surface roughness on adhesion, proposing a modified van der Waals force depending only on the radius of asperities. Two geometrical models were used in their study. One model is the same as the Rumpf model, ignoring the contact forces and considering only non-contact forces. The other model assumes the asperity is a small particle between two large spheres and was called the sandwich model. It is concluded that if the radii of surface asperities are smaller than 10 nm, the surface could be treated as smooth which contradicts with the experimental observation in the present work that even 1-2 nm roughness causes a sharp drop in adhesion force.

Electrostatic adhesion related to contact electrification, that is the transfer of charge during sample separation was not observed during most experiments. The reasons it was not observed significantly in this study may be as follows: 1) The silicon surface was oxidized and, therefore, was similar to the silica surface (sphere). Transfer of charge occurs only between dissimilar surfaces [Hor92], while the adhesion between similar surfaces determined by van der Waals forces; 2) Strong electrification occurs only in dry nitrogen, while our measurements were conducted in air with 25% relative humidity. It is possible that the adsorbed layer of water at the silica surface for

this humidity results in discharge and prevents formation of the electrical potential difference between the samples.

In conclusion, the adhesion force between a smooth flat silicon surface and a spherical glass surface in dry air can be explained by van der Waals force if we consider an intermolecular distance of about 0.3 nm. This force for rough solids can be calculated in the framework of Rumpf's approach, using contact and non-contact van der Waals forces. However, a more correct geometric model for the roughness profile should be used instead of the geometric model suggested by Rumpf.

Profiles, suggested in the present paper, provides calculation of correct adhesion forces by using only experimental geometric parameters, RMS and the wavelength λ.

The dependence F/R vs. RMS was found to have a different character for large and small radii R (sphere or tip) of samples. For R= 10 μm, a sharp decrease, nearly 10 times, was observed when the RMS increases from 0 to 2 nm. For R= 0.1 μm, the experimental decrease of adhesion force was only 1.5 times for the same values of RMS. The higher experimental values of F_{ad} for a tip with radius R=0.1 μm can be attributed to the interaction of the tip with several asperities rather than with one peak.

The Role of Velocity of Particles

As mentioned earlier, an effective collision environment is required to separate secondary particles by imparting enough forces on agglomerates in MAIC process or in any other dry processing techniques. In particular, tangential forces are needed to cause a small relative motion called slip over part of the contact points. By the action of shear forces, agglomerated secondary particles are spread over primary surface. For all impacts, the work done by the tangential force is twofold: work done in shear at the contact and work done in rotating the spheres [Tho91].

The magnetic particles were found to have rotational speeds 75-100 rev/sec depending on the frequency of the magnetic field. This high spinning was only detectable by enhanced image processors such as a high speed camera. The rotational movement of magnetic particles causes shear stresses or tangential forces during impact which breaks and spreads the agglomerates. The process is schematically drawn in figure 5-17. Due to creation of such shear forces on agglomerates by rotational movement, the surface coverage of PMMA primaries was increased significantly by increasing rotational speed of magnetic particles. The surface coverage

for 5 minute MAIC treated PMMA/alumina system as a function of rotation speed is shown in figure 4-21.

As explained earlier, tangential forces also causes detachment of secondaries. Savkoor and Briggs [Sav77] extended JKR theory to account for the effect of tangential forces. It was reported that the contact radius is decreased under increasing tangential force. After a critical force, a stable and continuous peeling was reached indicating that the work of adhesion cannot absorb the rate of energy release through detachment. The effect especially seen after a uniform and highly covered surface is obtained where the energy of impaction starts going to the detachment process rather than agglomerate breakdown.

The tangential force is a result of the velocity and impact of particles. Therefore, detachment dominates at a certain critical velocity, which is called the critical shear velocity. There are many studies on the determination of critical velocities using different substrate particle combinations [Wal90, Dah75, Sol94]. Soltani et al. evaluated the critical velocities as a function of particle size according to DMT and JKR models using copper particles and copper substrate as shown in figure 5-18. As can be seen from the figure the critical velocity for detachment for submicron range particles is around 10^5 cm/sec. In MAIC process the

translational and rotational velocities are measured around 35-60 cm/sec and 75-100 rev/sec which means that secondary particles or primary particles have velocities under the critical detachment regime. Therefore it can be concluded that MAIC process works in adhesion dominating region as far as the velocity of particles are concerned. On the other hand as the particle size or agglomerate size increases to 10 μm levels, the detachment velocities reduces to 100 cm/sec levels which is comparable to velocity in MAIC process.

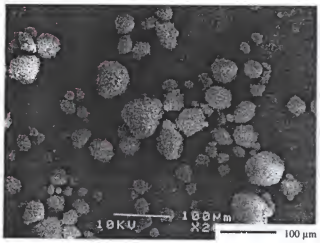

Figure 5-1. As received Al_2O_3 secondary particles.

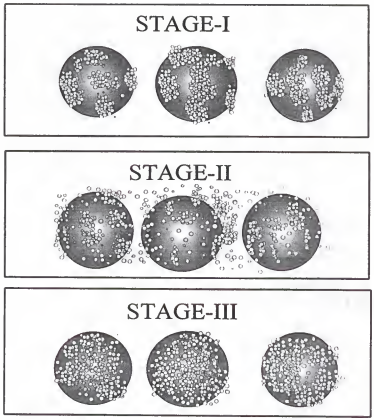

Figure 5-2. Schematic description of the stages of MAIC process.

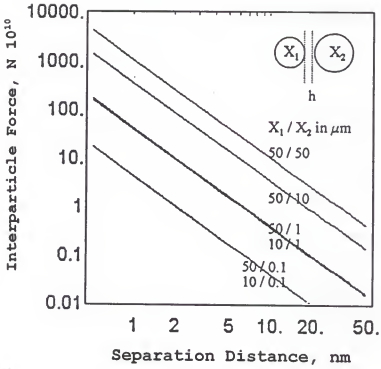

Figure 5-3. The effect of change in size of secondary particle on adhesion force based on vdW equation.

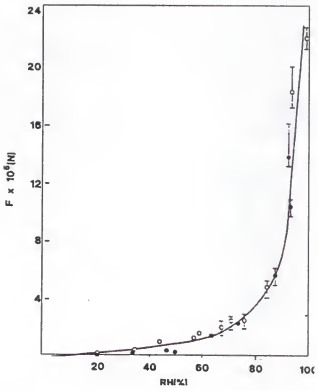

Figure 5-4. Variation of adhesion force with relative humidity for a glass/glass system [Har96].

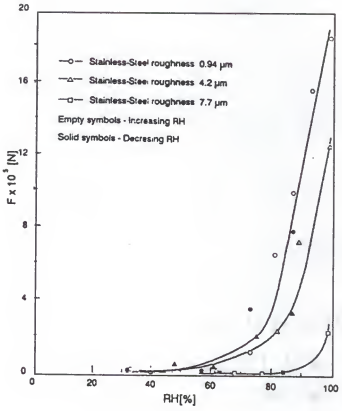

Figure 5-5. The effect of surface roughness on the adhesion force at varying humidity levels.

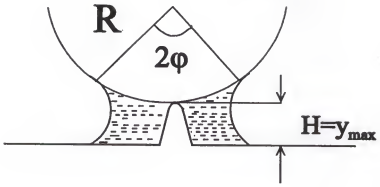

(a)

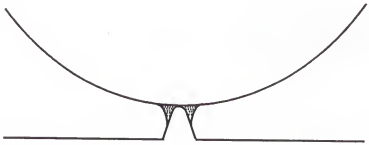

(b)

Figure 5-6. Liquid bridge a) $2r>y_{max}$ b) $2r<y_{max}$.

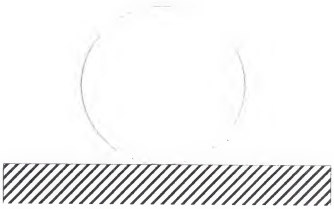

(a)

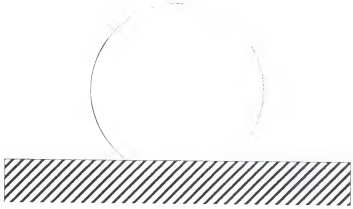

(b)

Figure 5-7. Schematic of contact region a)elastic b)plastic deformation cases.

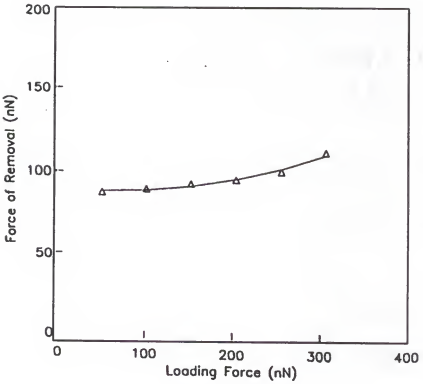

Figure 5-8. Force of removal for a 5 μm polystyrene sphere as a function of loading force.

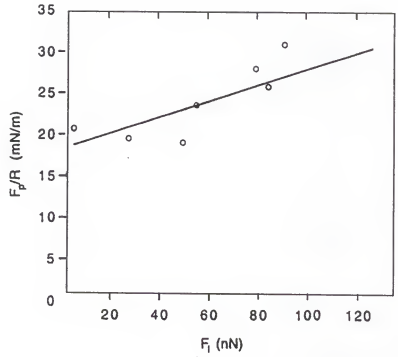

Figure 5-9. The variation of adhesion force with loading force for silica/iron oxide system.

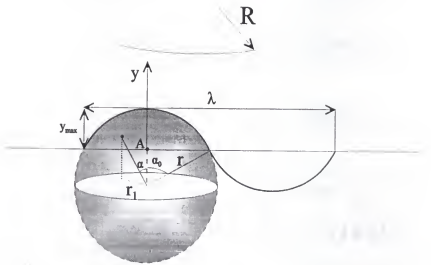

Figure 5-10. Long wave profile for description of roughness.

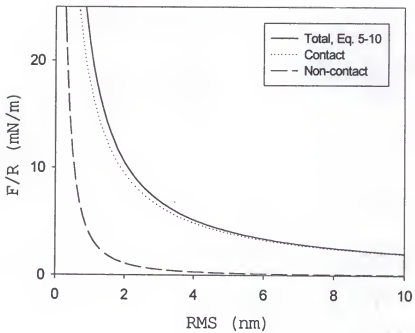

Figure 5-11. Theoretical dependence of adhesion force and its components on RMS according to equation (5-10). Contact and non-contact forces are the first and second terms of equation. Radius of sphere is 10 μm and the wavelength λ=250 nm.

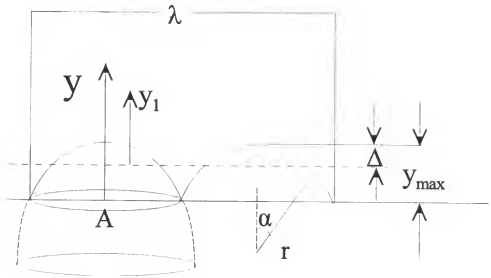

Figure 5-12. Roughness profile with bumps. Dashed line is an ideal boundary of surface.

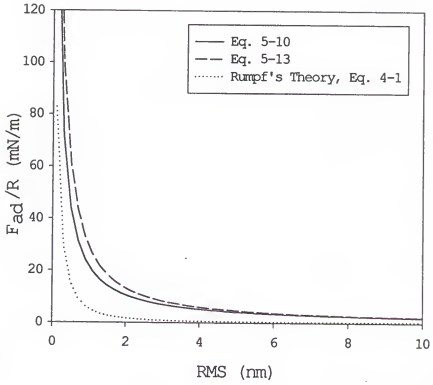

Figure 5-13. Theoretical dependence of adhesion force on RMS for equations (5-10) and (5-13). R=10 μm and λ=250 nm.

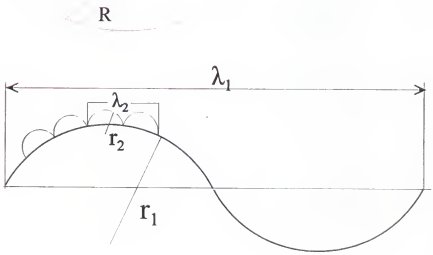

Figure 5-14. Double wave model for roughness profile.

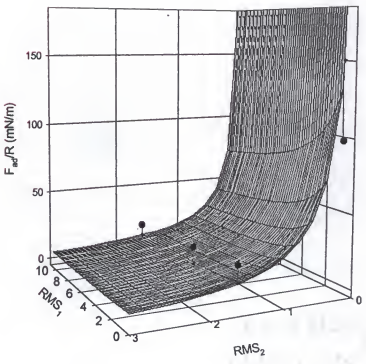

Figure 5-15. Comparison of experimental and theoretical results for adhesion force (equation 5-16) vs roughness measurements for the interaction between sphere (R=10 μm) and wafer surface.

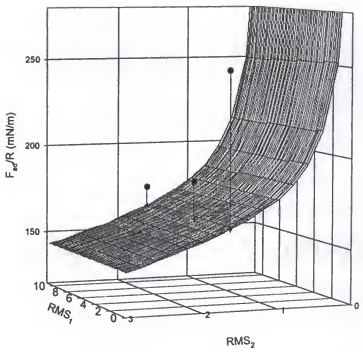

Figure 5-16. Comparison of experimental and theoretical results for adhesion force (equation 5-16) vs roughness measurements for the interaction between the cantilever tip (R=0.1 μm) and wafer surface.

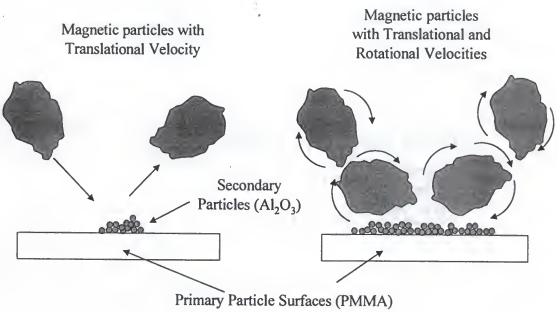
Magnetic particles with Translational Velocity
Magnetic particles with Translational and Rotational Velocities
Secondary Particles (Al_2O_3)
Primary Particle Surfaces (PMMA)

Figure 5.17. The interaction of magnetic particles during MAIC process.

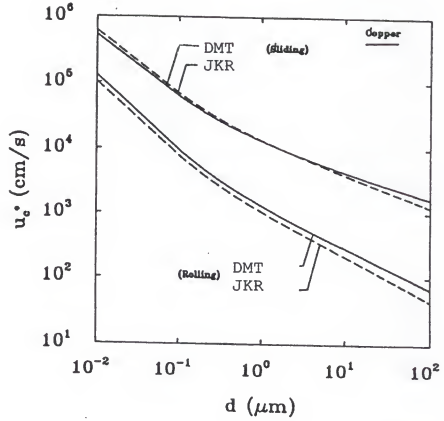

Figure 5-18. Critical shear velocity as a function of particle size for Cu particles.

CHAPTER 6
CONCLUSION

Composite particles were synthesized with a novel type dry technique, Magnetically Assisted impaction Coating, with a uniform surface coverage. The technique uses mechanical forces resulting from impaction of particles and has short processing times. The method is more practical than the existing technologies such as Mechanofusion, Hybridizer in terms of less equipment cost and simplicity. The use of low humidity and pressures as low as 700 mTorr improves the efficiency of process by improving fluidization in the system and adhesion of secondary particles. The size of secondary particles plays an important role in the process and was found to be below 0.4 μm to obtain an efficient coating.

Adhesion of particles is provided mainly by van der Waals forces at dry environments and capillary forces at humid environments. The transfer from "humid" to "dry" takes place near 60% RH. Significant difference exists in the magnitude of adhesion forces in dry and humid environments only for relatively smooth surfaces indicating the difficulty of liquid bridge formation on rough surfaces. The meniscus forms near

the contact peaks of interacting solids rather than the surfaces.

Adhesion force was observed to decrease sharply within 1-2 nm increase in roughness which could not be sufficiently explained with existing models. A model explaining adhesion behavior for nano-scale deviations from ideal smooth surface was developed defining roughness with wavelength and height of the asperity peak both are experimentally measurable parameters.

Plastic deformation at the contact region was observed to improve adhesion up to 2-3 orders of magnitude depending on the yield strength of the contacting bodies. The contribution of elastic deformation to adhesion was negligible. However, when the adhesion in humid environment is concerned elastic deformation flattens the asperity peaks and promotes liquid bridge formation and hence capillary forces particularly for soft bodies.

APPENDIX

The origins of the cartesian and spherical coordinate system are called as A and O, respectively. The projection r_1 of the peak radius r is:

$$r_1=r\sin\alpha \tag{1}$$

$$y=r(\cos\alpha+\cos\alpha_0) \tag{2}$$

For small angles $\alpha<<1$

$$r_1=r\alpha \text{ and } y=r/2(\alpha_0^2-\alpha^2) \tag{3}$$

Here $\alpha_0=\arcsin(\lambda/4r)=\lambda/4r$

The value of peak height, y_{max} can be calculated from equation as:

$$y_{max}=r\alpha_0^2/2=\lambda^2/32r \tag{4}$$

If we assume that y_{max} is a function of RMS as:

$$y_{max}=k_1RMS \tag{5}$$

$$r=\lambda^2/(32k_1RMS) \tag{6}$$

According to general definition:

$$RMS^2 = \int_0^{\lambda/4} \frac{y^2 2\pi r}{\pi(\lambda/4)^2} dr \; k_p \tag{7}$$

Here k_p is the surface packing density, maximum value of which for hexagonal packed spheres is 0.907. Substituting equations (1) and (2) in (7), $RMS=0.0172\lambda^2/r$ is obtained. Using equation (6), the roughness coefficient k_1 is calculated as $k_1=1.817$.

The height of the peak from equation (5.13) is then equal to:

$y_{max}=$ 1.817 RMS.

LIST OF REFERENCES

Alo88 Alonso, M., Satoh, M., and Miyanami, K., Powder Tech. 56,135 (1988).

Alo89a Alonso, M., Satoh, M., and Miyanami, K., Powder Tech. 59,65 (1989).

Alo89b Alonso, M., Satoh, M., and Miyanami, K., Powder Tech. 59,45 (1989).

Bha78 Bhattacharya, S., and Mittal, K.L., Surface Tech. 7,413 (1978).

Bhu95 Bhushan, B., Israelachvili J.N., and Landman, U., Nature, 374, 607 (1995).

Bow85 Bowling, R.A., J.Electrochem. Soc. 132, 2208 (1985).

Bow88 Bowling, R.A., *Particles on Surfaces I*, Ed. by Mittal, K.L.(Plenum Press, New York, 1988, p129).

Bra36 Bradley, R.S., Trans. Faraday Soc. 32, 1088 (1936).

Bra92 Brach, R.M.,and Dunn, P.F., Aerosol Sci. & Tech. 16, 51 (1992).

Bri94 Briscoe, B.J., and Panesar, S.S., J.Adhesion Sci. Tech. 8, 1485 (1994).

Chi84 Chikazawa, M., Kanazawa, T., and Yamaguchi, T., Kona 2, 54 (1984).

Coe78 Coelho, M.C., and Harnby, N., Powder Tech. 20, 201 (1978).

Cor66 Corn, M., *Aerosol Science*, Ed. by Davies, C.N. (Academic Press, London, 1966, p359).

Cot85 Cotaar, E.J.E.,and Rietema, K., J.Colloid & Interface Sci., 109,249 (1985).

Dah72 Dahneke, B., J.Colloid & Interface Sci.,40,1 (1972).

Dah75 Dahneke, B., J.Colloid & Interface Sci. 51,58 (1975).

Der75 Derjaguin, B.V., Muller, V.M., and Toporov, Y.P., J. Colloid and Interface Sci. 53, 314 (1975).

Don93 Donovan, R.P., Yamamoto, T., & Periasamy, R., Mat. Res. Symp. Proc. 315, 3 (1993).

Duc91 Ducker, W.A., Senden, T.J., and Pashley, R.M., Nature 353, 239 (1991).

Ful75 Fuller, K.N.G., and Tabor, D., Proc. Royal Soc. London A345,327 (1975).

Gan74 Gane, N., Pfaelzer, P.F., Tabor, D., Proc. Royal Soc. London A340,495 (1974).

Gel84 Geldart, D., Harnby, N., and Wong, A.C., Powder Tech. 37, 25 (1984).

Got95 Gotoh, K., Takebe, S., Masuda, H., and Banba, Y., Kona 191 (1995).

Ham37 Hamaker, H.C., Physica 4, 1059 (1937).

Har82 Harnby, N., and Jackson, I., *4th Europ. Conf. On Mixing* 173 (1982).

Har92 Harley, S., Thompson, D.W., and Vincent, B., Colloids & Surfaces 62, 163, (1992).

Har96a Harnby, N., Hawkins, A.E., and Opalinski, I., Trans IchemE, 74, 605 (1996).

Har96b Hartholt, G.P., Hoffmann, A.C., and Janssen, L.P.B.M., Powder Tech. 88, 341 (1996).

Her75 Hersey, J.A., Powder Tech. 11,41 (1975).

Her79 Hersey, J.A., Thiel, W.J., Yeung, C.C., Powder Tech. 24,251 (1979).

Hor92 Horn, R.G., and Smith, D.T., Science, 256, 362 (1992).

Iid93 Iida, K., Otsuka, K.D., and Sunada, H., Chem. Pharm. Bull. 41, 1621 (1993).

Isr82 Israelechvili, J.N., Fisher, L.R., Horn, R.G., and Christenson, H.K., *Microscopic Aspects of Adhesion & Lubrication,* Ed. by Georges, J.M. (Elsevier Sci. North Holland, 1982 , p55).

Isr85 Israelechvili, J.N.,*Intermolecular & Surface Forces,* (Academic Press, San Diego, 1985, p68).

Isr92 Israelechvili, J.N., Surface Sci. Reports 14, 109 (1992).

Joh71 Johnson, K.L., Kendall, K., and Roberts, A.D., Proc. Royal Soc. London A324,301 (1971).

Kaa95 Kaae, J.L., Mat. Res. Symp. Proc. 372, 139 (1995).

Kap98 Kapur, P.C., *Special Topics in Particle Science and Technology* ERC, Univ. of Florida (1998)

Kay97 Kaye, B.H., *Powder Mixing* (Chapman & Hall, London, 1997).

Kom94 Komatsubara, S., Isobe, T., and Senna, M., J. Am. Ceram. Soc. 77, 278 (1994).

Kru67 Krupp, H., Colloid Interface Sci. 1, 111 (1967).

Lac54 Lacey, P.M.C., J. Applied Chem. 4, 257 (1954).

Lif56 Lifshitz, E.M., Sov. Phys. JETP. 2, 73 (1956).

Mau84 Maugis, D., and Pollock, H.M., Acta Metall 32, 1323 (1984).

Miz91 Mizota, K., Fujiwara, S., & Senna, M., Materials Sci. & Eng. B10, 139 (1991).

Mul80 Muller, V.M., Yushenko, V.S., and Derjaguin, B.V., J.Colloid Interface Sci. 77, 91 (1980).

Mul83 Muller, V.M., Yushenko, V.S., and Derjaguin, B.V., J.Colloid Interface Sci. 92, 92 (1983).

Nai93a Naito, M., Kondo, A., and Yokoyama, T., ISIJ International 33, 915 (1993).

Nai93b Naito, M., Yoshikawa, M., Tanaka, T., and Kondo, A., Kona, 11, 229 (1993).

Ono89 Ono, K., Powder Sci. & Eng. 21, 83 (1989).

Pod94 Podczeck, F., Newton, J.M., and James, M.B., J. Adhesion Sci. Tech. 8, 1459 (1994).

Ran87 Ranade, M.B., Aerosol Sci. & Tech. 7, 161 (1987).

Rum75 Rumpf, H., *Particle Technology* (Chapman & Hall, New York, 1975, p118).

Rum78 Rumpf, H., Schubert, H., *Ceramic Processing Before Firing* Ed. by Onoda, G.Y. (J.Wiley & Sons, New York, 1978, p357).

Sav77 Savkoor, A.R., and Briggs, G.A.D., Proc. Roy. Soc. London A356, 103 (1977).

Sch94 Schmidt, A.R., and Walter, P., Metalloberflache 48, 260 (1994).

Sch94 Schaefer, D.M., Carpenter, M., Reifenberger, R., DeMejo, L.P., and Rimai, D.S., J.Adhesion Sci. & Tech 8, 197 (1994).

Sch95 Schaefer, D.M., Carpenter, M., Gady, B., Reifenberger, R., DeMejo, L.P., and Rimai, D.S., *Fundamentals of Adhesion and Interfaces*, Ed. by Rimai, D.S., DeMejo, L.P., and, Mittal, K.L. (VSP, New York, 1995, p35).

Sen97 Senna, M., Colloids and Surfaces A127, 257 (1997).

Sev97 Seville, J.P.K., Tuzun, U., Clift, R., *Processing of Particulate Solids* (Backie Academic & Professional, London, 1997, p115)

Sol94 Soltani, M and Ahmadi, G., J. Adhesion Sci. & Tech. 8, 763 (1994).

Ste80 Stephenson, P.L., Thiel, W.J., Powder Tech. 25, 115 (1980).

Sug98 Sugai, I., Jpn. J. Appl. Phys. 37, 257 (1998).

Tab77 Tabor, D., J. Colloid & Interface Sci. 109, 1 (1977).

Tan90 Tanno, K., Kona, 8, 74 (1990).

Tho91 Thornton, C., Yin, K.K., Powder Tech. 65, 153 (1991).

Tsa90 Tsai, C., Pui, D.Y.H., Liu, Y.H., Aerosol Sci. & Tech. 12, 497 (1990).

Tsa91 Tsai, C., Pui, D.Y.H., Liu, Y.H., Aerosol Sci. & Tech. 15, 239 (1991).

Tur74 Turner, G.A., Balasubramanian, M., Powder Tech. 10, 121 (1974).

Xie97 Xie, H.Y., Powder Tech. 94, 98 (1997).

Van74 Van Bree, J.L.M., Poulis, J.A., Verhaar, B.J., Schram, K., Physica 78, 187 (1974).

Vis89 Visser, J., Powder Tech. 58, 1 (1989).

Wal90 Wall, S., Walter, J., and Wang, H., Aerosol Sci. & Tech. 12, 926 (1990).

Wan96 Wang, C.M., J. Materials Sci. 31, 4709 (1996).

Wen36 Wenzel, R.N., Ind.Eng.Chem. 28, 988 (1936).

Zim63 Zimon, A.D., Kolloid Zh. 25, 317 (1963).

Zim82 Zimon, A.D., *Adhesion of Dust & Powder* (Consultants Bureau, New York, 1982).

BIOGRAPHICAL SKETCH

Ali Ata was born on March 22, 1966, in Istanbul, Turkey. He finished high school in the same city, in 1983. He obtained his bechelor of Science degree in Metallurgical Engineering from the Middle East Technical University, in 1989. He obtained his Master of Science degree from the Technical University of Istanbul in 1992. He started his Ph.D program at the University of California, San Diego in 1994. He transferred to the University of Florida in 1995. He continued his Ph.D work at this university in materials science with a specialty in electronic materials.

I certify that I have read this study and that in my opinion it conforms to acceptable standards of scholarly presentation and is fully adequate, in scope and quality, as a thesis for the degree of Doctor of Philosophy.

Rajiv K. Singh, Chair
Professor of Materials
Science and Engineering

I certify that I have read this study and that in my opinion it conforms to acceptable standards of scholarly presentation and is fully adequate, in scope and quality, as a thesis for the degree of Doctor of Philosophy.

Robert DeHoff
Professor of Materials
Science and Engineering

I certify that I have read this study and that in my opinion it conforms to acceptable standards of scholarly presentation and is fully adequate, in scope and quality, as a thesis for the degree of Doctor of Philosophy.

John J. Mecholsky
Professor of Materials
Science and Engineering

I certify that I have read this study and that in my opinion it conforms to acceptable standards of scholarly presentation and is fully adequate, in scope and quality, as a thesis for the degree of Doctor of Philosophy.

Laurie A. Gower
Assistant Professor of
Materials Science and
Engineering

I certify that I have read this study and that in my opinion it conforms to acceptable standards of scholarly presentation and is fully adequate, in scope and quality, as a thesis for the degree of Doctor of Philosophy.

Bhavani V. Sankar
Professor of Aerospace
Engineering, Mechanics,
and Engineering Science

This dissertation was submitted to the Graduate Faculty of the College of Engineering and to the Graduate School and was accepted as partial fulfillment of the requirements for the degree of Doctor of Philosophy.

December, 1998

Winfred M. Phillips
Dean, College of
Engineering

M. J. Ohanian
Dean, Graduate School

I certify that I have read this study and that in my opinion it conforms to acceptable standards of scholarly presentation and is fully adequate, in scope and quality, as a thesis for the degree of Doctor of Philosophy.

Bhavani V. Sankar
Professor of Aerospace
Engineering, Mechanics,
and Engineering Science

This dissertation was submitted to the Graduate Faculty of the College of Engineering and to the Graduate School and was accepted as partial fulfillment of the requirements for the degree of Doctor of Philosophy.

December, 1998

Winfred M. Phillips
Dean, College of
Engineering

M. J. Ohanian
Dean, Graduate School